Morphometric evidence of 3.6 Ga glacial valleys and glacial cirques in martian highlands: South of Terra Sabaea

Axel Bouquety, Antoine Séjourné, F. Costard, Denis Mercier, Sylvain Bouley

Version of Record: https://www.sciencedirect.com/science/article/pii/S0169555X1930056X
Manuscript_580742b4d52830921c428cb620b52c04

Morphometric evidence of 3.6 Ga glacial valleys and glacial cirques in martian highlands: south of Terra Sabaea

Axel Bouquety[a*], Antoine Sejourné[a], François Costard[a], Denis Mercier[b] & Sylvain Bouley[a]

[a] *GEOPS, Univ. Paris-Sud, CNRS, Université Paris-Saclay, Rue du Belvédère, Bât. 504-509, 91405 Orsay, France*

[b] *Sorbonne Université , 191 rue Saint Jacques 75005, Paris, France*

**Corresponding author. E-mail address: a.bouquety@gmail.com (A.Bouquety).*

Abstract

The climate of early Mars remains unclear and the debate is topical. Recently, climatic models have suggested a cold climate during the Noachian/ Early Hesperian on Mars, which goes against the wet and warm climate often put forward. The purpose of this study is to seek geomorphologic evidence of this early cold climate. To achieve this, a step-by-step study of the geometry and morphology of several martian valleys has been done in the southern highlands. The analysis highlights the morphometric properties which enable the identification of martian glacial landscapes. We identified 100 cirques and 83 glacial valleys in two craters and on one mountain in the southern part of Terra Sabaea. The studied morphologies have the same morphometric characteristics and trends as terrestrial and martian glacial valleys and glacial cirques. In contrary, these trends are very different from those observed in fluvial valleys on Earth and on Mars. (1) The martian glacial valleys are U-shaped with a large flat floor and a V-index > 0.20. While martian and terrestrial fluvial valleys are V-shaped with a V-index < 0.1. (2) The length to width ratio is >1 while for fluvial valleys this ratio is $>>1$. (3) Finally, the cross-sectional area and the elevation are higher for the glacial valleys compared to the fluvial ones. These glacial valleys often originate with a topographic hollow which have the same properties than terrestrial glacial cirque. The glacial landscapes identified in southern Terra Sabaea are restricted to elevations $>$ 1000 m and are dated by crater counting to be 3.6 Ga. This study strongly supports glacial processes as the origin of these valleys and cirques, and is the first morphometric evidence of glacial valleys associated with glacial cirques in the southern highlands in agreement with the climatic models. We propose that the martian climate during the late Noachian/early Hesperian was characterized by glaciated highlands at elevations greater than 1500 m and at lower elevations where fluvial valley network has been identified ($<$1500 m) the climate was more temperate allowing liquid water to be stable and creating fluvial valley

networks.

Keywords: Glacial landscape, Late Noachian/Early Hesperian, Morphometry, Early Mars.

---

1. Introduction

The presence of valley network is one of the best lines of evidence for prolonged surface water on Mars, and they are located preferentially in the southern highlands. These valleys have V-shaped or U-shaped cross-profile shapes and commonly include inlet and outlet valleys of Noachian-aged basins (Fassett and Head, 2008b). The valleys width ranges is from 50 m to 10 km, their median depth is 80 m and their length is usually less than few hundred kilometers. The origin of the valley networks remains uncertain and four hypotheses are proposed: (1) precipitation-fed surface runoff (Craddock and Howard, 2002); (2) runoff fed by surface ice melting (Segura, 2002); (3) runoff fed by surface or near surface melting by magmatic intrusions (Gulick, 2001); (4) sapping from subsurface aquifers (Carr, 1995). Whatever their formation process(es), the presence of valley networks similar to those on Earth (Baker, 2001; Hynek et al., 2010), clay minerals (Bibring et al., 2006), lakes, alluvial fans, and deltas (Ramirez and Craddock, 2018) show that during the Noachian (4.5-3.7 Ga), a hydrosphere was active on the surface of Mars with relatively warm and wet conditions. Some of these valley networks, are dated to the early Hesperian around 3.6 Ga (Fassett and Head, 2008a; Bouley. and Craddock, 2014). During the Hesperian, there was the formation of outflow channels (Carr and Malin, 2000). The abrupt emergence of outflow channels into the landscape indicates a formation by the rapid release of large volumes of water stored as subsurface groundwater or as an aquifer under pressure (Carr and Head, 2010). In addition, the observed surface alteration products changed, the Noachian clays gave way to sulfates from the late Noachian to the Hesperian, which indicates a global change in the aqueous chemistry of Mars (Bibring et al., 2006). These mineralogical and geomorphological lines of evidence show that the active Noachian hydrosphere lost its intensity and changed to a cryosphere during the Hesperian (Carr and Head, 2010).

Currently, the distribution of valley networks appears to be controlled by the topography induced by the Tharsis dome. Based on this correlation, Phillips (2001) suggested that the valley networks were formed after the formation of Tharsis, during the Noachian. However, recent geodynamic modeling showed that without Tharsis, the valley networks would have the same distribution as observed today, in a south tropical band from 40°S to 0°S (Bouley. et al., 2016). The growth of the Tharsis dome started during the Noachian era

(more than 3.7 billion years ago). Its position has induced a reorientation of the planet with respect to its spin axis (true polar wander, TPW), which is responsible for the present equatorial position of the volcanic province (Bouley. et al., 2016). It has been suggested that the Tharsis load on the lithosphere affected the orientation of the valley networks (Bouley. et al., 2016). Moreover, climate modeling has shown that with Noachian/ early Hesperian conditions, with an atmospheric pressure less than 1 bar, a reduced Tharsis bulge topography, and an obliquity of 45°, there is a preferential deposition of ice in the southern highlands in the same area as the valley networks (Wordsworth et al., 2013; Bouley. et al., 2016). This globally sub-zero scenario called "icy-highlands" for the late Noachian climate may be sufficient to explain most of the fluvial morphology and geology without the need to invoke additional long-term warming mechanisms or an early warm and wet Mars (Wordsworth et al., 2013; Head and Marchant, 2014). Therefore, it is postulated that the valley networks could have been formed in a cold climate.

So, on the one hand, several studies invoke a wet and warm climate allowing the formation of the valley networks (Carr, 1995; Craddock and Howard, 2002; Bibring et al., 2006; Carr and Head, 2010). And on the other hand, the new models invoke the "icy-highlands" scenario for early Mars (Wordsworth et al., 2013; Bouley. et al., 2016).

The purpose of this study is to seek geomorphologic evidence of this hypothesised cold climate in the southern highlands. To achieve this, we studied an area in Terra Sabea where ice should have been accumulated according to the models (Wordsworth et al., 2013; Bouley. et al., 2016). We performed a comparison between morphologies found in this area and those found in previously studied martian and terrestrial glacial and fluvial valleys. By studing the geometry and the morphology of the features we can deduce whether the origin of the valleys is liquid water or flowing ice.

2. Glacial landforms on Earth and Mars

2.1. Characteristics of glacial landforms on Earth

Glacial landforms can be recognized based on their geometry and morphology. Penck (1905) and de Martonne (1910) were the first to compare the morphology of alpine glacial valleys with fluvial valleys. Firstly, the study of glacial valleys revealed that their morphometry is very different from fluvial valleys (Section 4.2). Secondly, it showed that glacial valleys are often associated with other stuctures characteristic of glacial activity. These valleys are characterized by an accumulation of snow at the valley head forming a cirque. The

snow then compacts and sinters to ice, and by the action of gravity the ice mass flows down the slope above the equilibrium line, the accumulation zone. Below the equilibrium line, the glacier enters in the ablation zone. Here, the ice melts and/or sublimates and meltwater and sediment are delivered on the proglacial plains (Bennett and Glasser, 2011). The deposital features created are: (1) moraines resulting from debris entrained during glacial erosion that are transported and deposited at the glacier side and/or the glacier front when the glacier is stable and then retreats. The frontal moraine indicates the maximum advance of the glacier (Andersson, 1998; Ewertowski and Tomczyk, 2015). (2) Eskers which are a type of straight-to-sinous ridge composed of sand and gravel resulting from the flow of glacial meltwater in predominantly subglacial and englacial conduits (Bennett and Glasser, 2011). Eskers are generally formed under warm-based glaciers, the core being formed in a tunnel inside the ice (Brennand, 2000). At and beyond the margin of the glacier, ice blocks buried in the esker will melt and form (3) kettle holes (Fitzsimons, 1991). Kettle hole are enclosed topographic depression that is formed at the surface of outwash deposits in recently deglaciated surface (Corti et al., 2012).

This landform assemblage, making up a classic glacial landscape, is composed of a glacial cirque, a glacial valley, and associated deposits. This assemblage is found in regions which have experienced glacial activity, and their distributions is linked to paleoclimate (Barr and Spagnolo, 2015).

2.2. Past and recent martian glaciations

Evidence of past glaciations have been extensively reported on Mars. In the southern hemisphere, at latitudes higher than 30°, some craterwall valleys have been interpreted as glacial valleys in two Noachian-aged craters and in one Hesperian-aged crater (Hobbs et al. 2016; Fig. 1). These glacial valleys exhibit a U-shaped cross-section and a length to width ratio >1 while fluvial valleys have a length to width ratio $>>1$ (Hobbs et al., 2016). In addition, evidence of old glacial landsystem (3.5 Ga) in Ius Chasma and Central Candor Chasma in Valles Marineris have been identified using paraglacial structures (Mège and Bourgeois, 2011; Gourronc et al., 2014).

Evidence of Amazonian glaciation has been extensively reported in the mid-latitudes. This takes the form of viscous flow features (VFF) that often appear on the slopes of high-relief features and exhibit morphologies indicative of glacial viscous flow (Souness and Hubbard, 2012). They are elongated flow-like features composed of essentially pure glacial ice below a protective layer of debris (Holt et al., 2008; Plaut et al., 2009). VFF

can be divided into three types: (1) glacier-like forms (GLF) are visually similar to terrestrial valley glaciers, showing signs of downpositive relief viscous deformation (Hubbard et al., 2014) (2) lobate debris aprons (LDA) are characterized by lobate features surrounding massifs and are often observed at the base of crater walls, in that case it is call concentric crater fill (CCF; Squyres 1979) (3) lineated valleys fills (LVF) are formed on valley floors from the convergence of two or more LDA-type flows (Squyres, 1979). Finally, previous work has reported deposit features similar to terrestrial eskers (Kargel and Strom, 1992; Fastook et al., 2012; Gallagher and Balme, 2015; Butcher et al., 2016) and moraines like-ridges (MLR) at the foot of many mid-latitude crater walls (Arfstrom and Hartmann, 2005; Conway et al., 2018). These landforms are in many cases similar to glacial landforms on Earth and allow analogue-based comparisons to be made (Souness and Hubbard, 2012).

3. Study area in Terra Sabaea

3.1. Description of the area

We focused our study on Terra Sabaea. Terra Sabaea is located northwest of Hellas planitia (Fig. 1a). This area is characterized by a high density of valley networks dated of the late Noachian/early Hesperian (Hynek et al. 2010; Bouley. and Craddock 2014; Fig. 1b). The majority of these valley networks are located in the inter crater plains, but some of them are located on the inner wall of impact craters in the study area (Fig. 2a). We noted that some valley-like features, unmapped by Hynek et al. (2010), could be found on both negative relief features, such as impact craters, but also on positive relief features, such as mountains (Fig. 2b,c,d). Terra Sabaea has a mean elevation of 1740 m and is located where ice is predicted to have been deposited in the Noachian according to the models described above (Wordsworth et al., 2013; Bouley. et al., 2016). To seek geomorphologic evidence for this hypothesised cold climate, we studied three sites: Dawes crater, an unnamed crater we called "crater 1" and a unnamed mountain we called "mountain 1" (Fig. 2).

3.1.1. Mountain 1

This feature is an isolated mountain 2 km high with a summit at 3.5 km in elevation above the MOLA reference datum. It is located 425 km to the northeast of Dawes crater (42°17'E, 2°55'S; Fig. 2a). The south

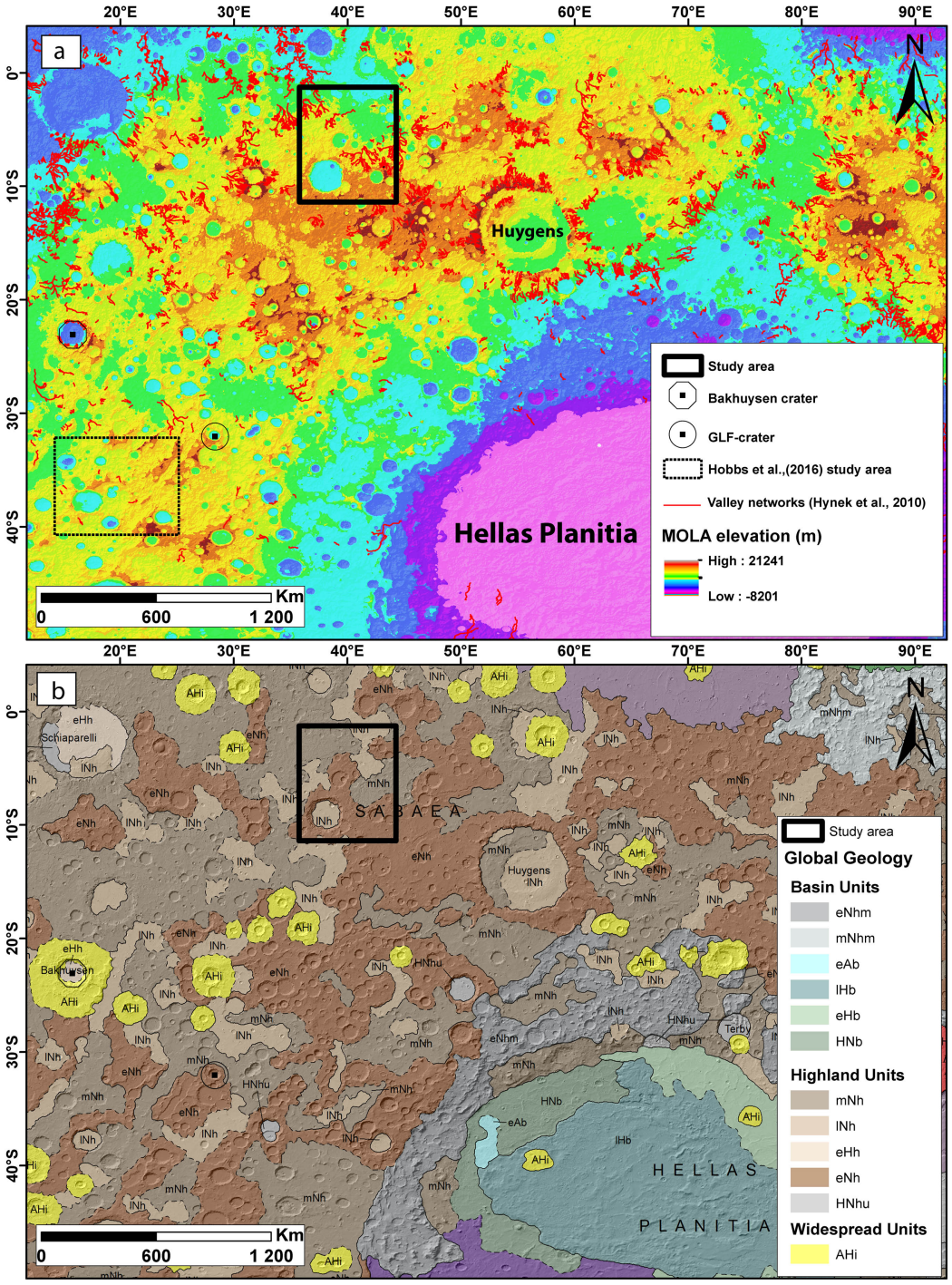

Fig. 1. Terra Sabaea and Noachis Terra in the southern highlands. (a) Study area and areas used for comparison. The red line represents the valley networks mapped by Hynek et al. (2010). Mars orbiter laser altimeter (MOLA) digital elevation background. (b) USGC geological map of the area (Tanaka, 2014). Images credit NASA/JPL/University of Arizona.

facing slope appears topographically bland and the north facing slope is dissected by valleys running from the summit to the base with lengths on the order of tens of kilometers (Fig. 2b).

3.1.2. Crater 1

This unnamed crater is located at 150 km to the east of Dawes crater (42°34'E, 9°10'S; Fig. 2a). It has a diameter of 74 km and a depth of 2 km. It is dated to the early Noachian (Tanaka, 2014). Its walls have some unmapped valleys of tens of kilometers in length (Fig. 2c).

3.1.3. Dawes crater

Dawes crater is a large impact crater (38°8'E, 8°55'S; Fig. 2a) with a diameter of 200 km, a depth of 2.5 km and has walls with steep inner slopes $> 20°$ (Fig. 2d). Its walls have 35 valleys mapped by Hynek et al. (2010) as valley networks, located on the southern wall (Fig. 2a). The northern wall has some unmapped valleys. Dawes crater is dated to the late Noachian (Tanaka, 2014).

4. Data and methods

4.1. Imagery

The purpose of the study is to define if the valleys in the study area are glacial or fluvial. To achieve this we compared the studied valleys with known cases on Earth and Mars. We used Context Camera image (CTX) with a resolution of 6 m/pixel (Fig. 3a; Malin and Edgett 2001) to characterize the valleys. This first step was the most important because it allowed us to identify the morphologies to be studied in more detail. Then, to constrain their geometry, we used the Digital Terrain Map Reduced Data Record (DTMRDR) data with 1 m numeric height resolution from High-Resolution Stereo Camera (HRSC) with a resolution of 10-20 m/pixel depending on the ground resolution of the respective image (Gwinner et al., 2016) and MOLA gridded global digital elevation data with a resolution of 1/64° in latitude x 1/32° in longitude (Fig. 3b; Smith et al. 2001). We made our measurements using ArcGIS software. The projection systems used was "SimpleCylindrical_Mars" for CTX, with this projection, distortion increases as the distance from the

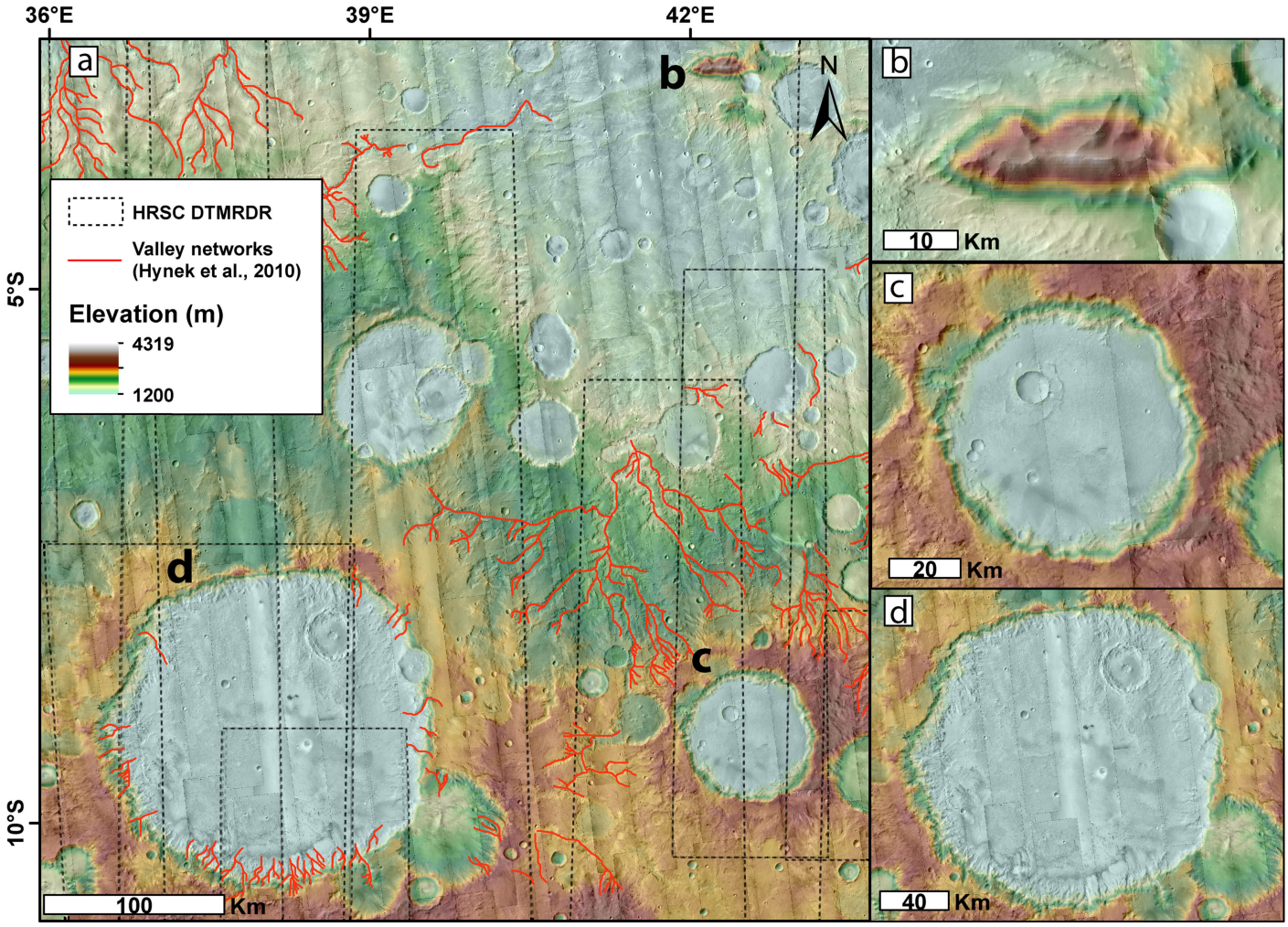

Fig. 2. Location of the three study areas. (a) Context camera (CTX) mosaic of the study area with MOLA digital elevation map. The red lines are the valley networks identified by Hynek et al. (2010) (b) Mountain 1 CTX images with MOLA background . (c) Crater 1 CTX images with MOLA background . (d) Dawes crater CTX images with MOLA background. All the images and data used are sum up in the supplementary (Table 3). Images credit NASA/JPL/University of Arizona.

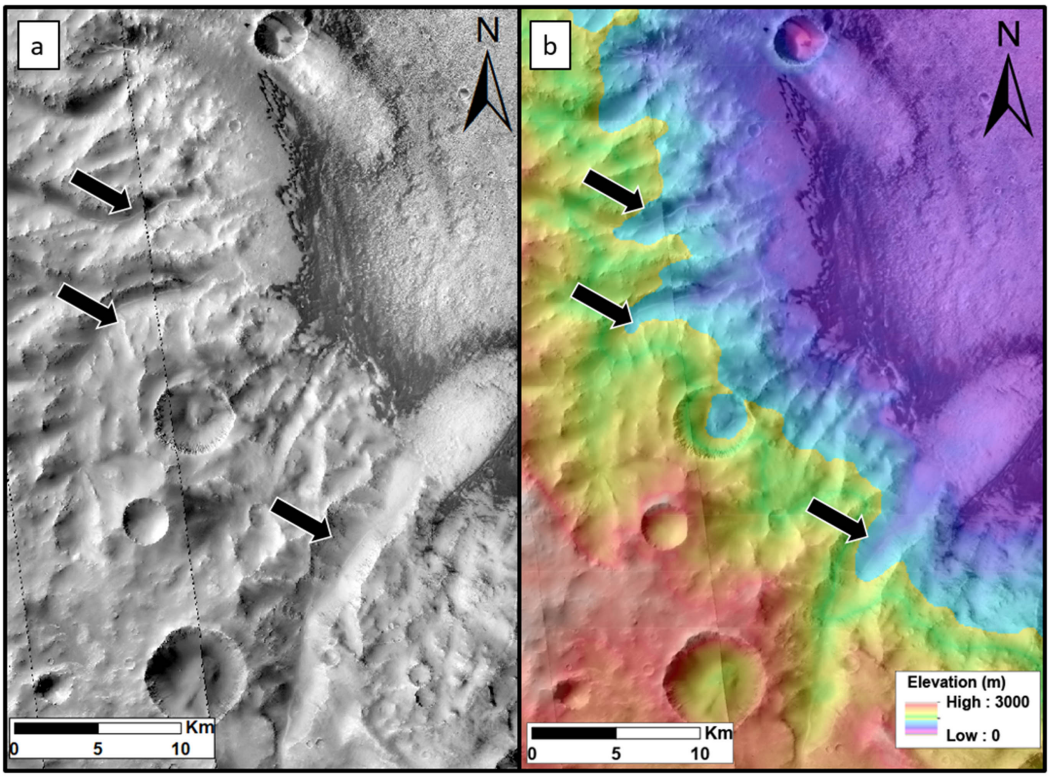

Fig. 3. Example of studied valleys. The west rim of Dawes crater visualised using (a) CTX images P11_005461_1706_XI_09S323W; P17_007742_1708_XN_09S323W (b) MOLA colorised data overlain on CTX images. The black arrows indicate the location of the valleys. Images credit NASA/JPL/University of Arizona.

standard parallels increases. We used "SINUSOIDAL_MARS" for DTMRDR, the scale along all parallels and the central meridian of the projection is accurate. And "Mars2000_ECylindrical_clon0" for MOLA. Our study areas are near the equator (between 2° and 9°S), which is a standard parallels so the distortions can be neglected. To measure valleys on Earth, we used data from the Institut national de l'information géographique et forestière (IGN). We used the 25m/pixel DEM.

4.2. Morphometrical analysis of terrestrial glacial landscapes

4.2.1. Terrestrial glacial and fluvial valleys

Penck (1905) showed that the cross-section area of alpine glacial valleys increases down to the equilibrium line and then decreases downstream to the end of the valley. This is the "law of adjusted cross-sections" (Penck, 1905). Since 1905, numerous authors have studied the morphological and geometrical differences between

fluvial and glacial terrestrial valleys using various parameters: length, width, slope, elevation, drainage area, and cross-section. The own properties of ice and liquid water (state of matter, velocity, rate of abrasion...) make that glacial valleys are different from fluvial valleys by the footprint they leave in the landscape. Generally, a glacial valley is U-shaped with a wide flat floor, steep walls and symmetric shoulders (Penck, 1905; Livers and Wohl, 2015). These characteristics come from the processes of glacial erosion: (1) Glacial quarrying is the means by which a glacier removes larger chunks and fragments from its bed and walls (Bennett and Glasser, 2009). (2) Glacial abrasion is the process by which rock particles transported at the base of a glacier are moved across a bedrock surface scratching and wearing it away (Bennett and Glasser, 2009). A fluvial valley is V-shaped with a narrow floor, gentle walls and symmetric shoulders (Montgomery, 2002; Livers and Wohl, 2015). These characteristics come from the process of fluvial erosion: (1) Water abrasion generate detachment of soil particles by flowing water under the influence of both drag and lift forces (Léonard and Richard, 2004). These differences of erosion have influences on morphology and geometry of these two kinds of valleys. Then, from literature, we created a list of morphological and geometrical characteristics that allow the distinction of glacial valleys from fluvial ones (Table 1).

4.2.2. Terrestrial glacial cirques

Terrestrial glacial valleys have often valley heads upstream where the ice accumulates. When these valley heads are a hollow, open downstream but bounded upstream by the crest of a steep slope a 'headwall' ($>27°$) which is arcuate in plan around a more gently sloping floor ($<27°$), They are called glacial cirqueIt is glacial if the floor has been affected by glacial erosion while part of the headwall has developed subaerially, and a drainage divide was located sufficiently close to the top of the headwall (the cirque crest) for little or none of the ice that fashioned the cirque to have flowed in from outside, (Barr and Spagnolo, 2015; Evans and Cox, 2017). The characteristics of cirques are readily measurable due to in the absence of ice and can include: (1) their spatial distribution, (2) the length (L), (3) the width (W), (4) the amplitude (A), (5) the height range (H), (6) the size ($\sqrt[3]{LWH}$), and (7) the axial gradient (arctan(A/L)). This parameter approximates the surface slope of a former glacier just filling the cirque (Barr and Spagnolo, 2015; Evans and Cox, 2017). Often, cirque size is calculated in order to assess whether cirques have developed isometrically (whether the rate of growth has been equal in all three orthogonal dimensions) or allometrically (whether the rate of cirque lengthening, widening and deepening has been unequal, and cirques have therefore changed shape

Morphology	**References**
Glacial valleys are U-shaped while fluvial valley are V-shaped	Roberts and Rood, 1984 Livers and Wohl, 2015
Glacial valleys have a wide flat floor unlike fluvial valley which are steeper	Penck, 1905 Montgomery, 2002
Glacial valleys have symmetric shoulders that delimit the drainage area	Montgomery, 2002 Livers and Wohl, 2015
Above the shoulders glacial valleys have a cirque-like niche	Penck, 1905 Barr and Spagnolo, 2015
Glacial valleys have a longitudinal profile which has a gentle slope with slope failures	Roberts and Rood, 1984 Augustinus, 1992
Glacial valleys have steeps walls unlike fluvial valleys which have gentle walls.	Penck, 1905 Livers and Wohl, 2015
Geometry	
Glacial valleys are wider than fluvial ones	Roberts and Rood, 1984 Augustinus, 1992 Livers and Wohl, 2015
The law of adjusted cross-sections	Penck, 1905
The elevation of glacial valleys is higher than fluvial one	Roberts and Rood, 1984 Montgomery, 2002
For drainage area > 50 km² the cross section ratio is four times bigger for glacial valley than for fluvial valleys	Montgomery, 2002

Table 1. Morphological and geometrical criteria used to distinguish fluvial and glacial valley in this study based on terrestrial studies.

during development; Olyphant 1981; Evans 2010). To assess this, length, width and altitudinal range are plotted against cirque size. They can provide information about the duration and intensity of the glacial conditions that formed them (Delmas et al., 2015).

4.3. Morphometrical analysis of valleys on Mars

We used all the criteria described in Table 1 and in Table 2 to study the mapped valley networks and unmapped valleys in our study area. Authors studying terrestrial landscapes generally use only three or four parameters to characterize valleys and emphasis is placed on the shape of the valley, U-shaped for glacial valleys and V-shaped for fluvial ones. The shape is an important indicator of the origin of the valley, but it is not always a discrimining parameter, for example, a V-shaped valley can be filled by deposits and become more U-shaped. In order to circumvent this problem, in this paper, we studied the morphometry of the martian valleys using as many parameters as possible to interpret the origin of the valleys.

4.3.1. Morphological identification of the valleys and their drainage area

The first step in the analysis was to define the outline of the studied valleys using two criteria: (1) The shoulders of the valley should be well preserved and should be continous over hundred of meters. As for terrestrial measurements, we chose to stop the valley when we can no longer follow the crest (Livers and Wohl, 2015). (2) The overall morphology should be the same along the whole length of the valley. For the valley networks, we do not consider the entire network as a single valley but as a set of tributary valleys. The shapefile thus obtained allowed us to define the outline of the valley, but also to obtain the drainage area within which the erosion (by ice or liquid water) took place (Fig. 4a).

4.3.2. Valley length and width

The length of the valley was defined using a longitudinal line extending from the furthest upstream part of the valley to the downstream part of the valley, sub-parallel to the valley shoulders (Fig. 4a). Then, in order to have a wide range of measurement, we divided the length into four segments of equal length. The width was measured at each segment boundary (5 width mesurements per valley), perpendicular to the length line and crossed the crest on each side of the valley (Fig. 4a).

Valley parameters	Abbreviation	Definition
Length (m)	L	Longitudinal line extending from the upstream part to the downstream part.
Width (m)	W	Perpendicular to the length line.
Slope (°)	Sl	Average values of all pixel in the valley shape.
Elevation (m)	El	Average values of all pixel in the valley shape.
Depth (m)	Dp	Difference between the highest and lowest point from a cross-sectional profile.
V-index (dimensionless)	V-index	Deviation from an ideal V-shaped valley.
Cross-section (m^2)	CS	Calculated from the cross-sectional profiles.
Length/width ratio (dimensionless)	L/W	Length/ width.
Valley head parameters		
Length (m)	L	Length of the median axis.
Width (m)	W	Maximum dimension measured perpendicular to the length line.
Amplitude (m)	A	Difference in altitude between the highest and lowest point on length line.
Heigth range (m)	H	Difference between the highest and lowest point.
Axial gradient (°)	Axgrad	Arctan(A/L).
Size (m)	S	$\sqrt[3]{LWH}$.
Length/height ratio (dimensionless)	L/W	Length/height.

Table 2. Parameters measured for the valleys and valley heads used in this study. Selected from several terrestrial studies (Johnson, 1904; Penck, 1905; de Martonne, 1911; Graf, 1970, 1976; Olyphant, 1981; Roberts and Rood, 1984; Augustinus, 1992; Montgomery, 2002; Amerson et al., 2008; Evans, 2010; Zemp et al., 2011; Barr and Spagnolo, 2015; Delmas et al., 2015; Livers and Wohl, 2015; Hobbs et al., 2016; Evans and Cox, 2017; Zimmer and Gabet, 2018).

4.3.3. Valley slope and elevation

The slope was calculated for every pixel of the HRSC DTMRDR that fell within the valleys using the ArcGIS tool "slope". Then to extract the average slope and elevation values for each valley we used the ArcGIS tool "extract by mask". This tool allow to compute the average values of all pixel that fell within the outline previously drawn for the valley (Fig. 4a-b).

4.3.4. Valley cross-sectional area and V-index

The cross-sectional area was calculated from the transverse profile at the start and end of each segment (0%, 25%, 50%, 75%, 100% of the valley length). The profile crossed the two shoulders of the valley. From this profile, we extracted the maximum depth of the valley (Fig. 4e). Five cross-sectional areas were calculated, one for each segment we measured, and the average valley cross-sectional area was calculated from these five values. In order to characterize the shape of the valleys we used the V-index (Zimmer and Gabet, 2018). This V-index is the measure of the deviation from an ideal V-shaped valley. It is calculated by comparing the valley cross-sectional area (Ax) between the valley bottom and a specified height above the valley floor to that of an ideal V-shaped cross-section with the same height and width as the subject cross section (Av, Zimmer and Gabet, 2018).

$$V - index = (Ax/Av) - 1 \tag{1}$$

When V-index = 0, the ideal V-shaped valley is the same that the mesuread one. If the valley is U-shaped the V-index > 0 whereas V-shaped valleys have a V-index < 0 (Zimmer and Gabet, 2018). We chose to calculate the V-index for each valleys at 50% of the valley length.

4.4. Morphometrical analysis of valley heads on Mars

Some valley heads on Mars have an theater-like form. For these valley heads we defined the outline, using the same method as described in section 4.3.1. Then, we measured its width and length (Fig. 4c). The altitudinal range was obtained by using the same method described previously for the valleys (Section 4.3.3; Fig. 4c,d,f). The amplitude was obtained by mesuring the difference in altitude between highest and lowest points on the length line (Evans and Cox, 2017). The size of the valley heads was calculated using the

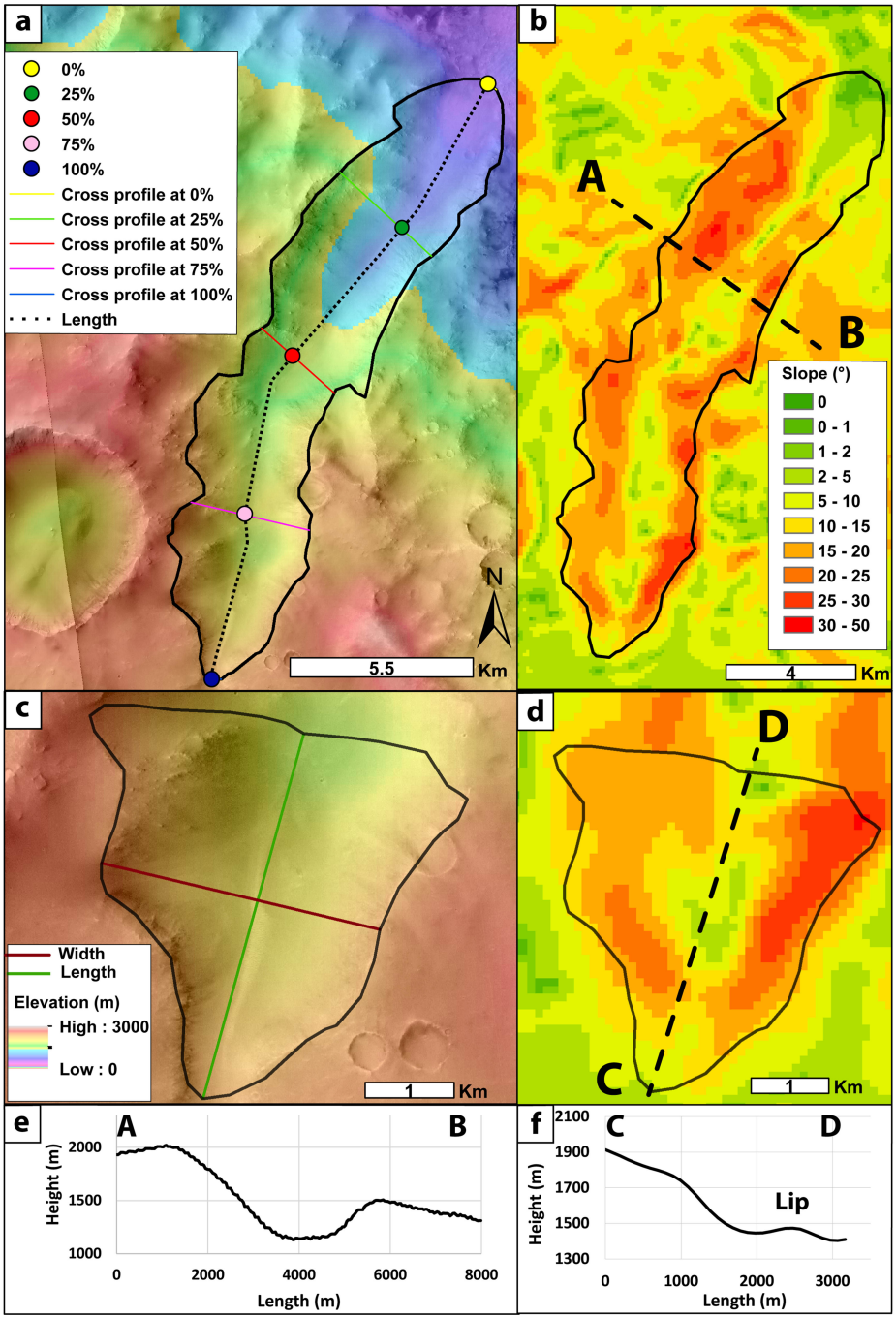

Fig. 4. Valley and valley head morphometric measurement. (a) A valley in Dawes crater and its associated valley head, where 0% correspond to the furthest point downstream and 100% the furthest point upstream. Background is CTX images (P17_007742_1708_XN_09S323W; P11_005461_1706_XI_09S323W) and MOLA elevation data. (b) Slope map of the valley in (a) (calculated from HRSC DTMRDR: h1950_0000_bl3) where the dashed line shows the position of the cross-sectional profile shown in (e). (c) Detailed view of the valley head shown in (a). (d) Slope map of the valley head, where the dashed line shows the position of the longitudinal profile shown in (f). Images credit NASA/JPL/University of Arizona.

relation

$$Size = \sqrt[3]{LWH} \tag{2}$$

(with L: Length, W: Width, H: Height), and the axial gradient using the relation

$$Axgrad = arctan(A/L) \tag{3}$$

(with A: Amplitude, L: Length). The boundary between the valley head and the valley is not always very clear. To be consistent between the different studied valleys, we chose to set this boundary to the change in topographic break in slope that marks the transition between the upstream valley head and the downstream main valley (Fig. 4f).

4.5. Comparative morphometrical analysis with known valleys on Earth and Mars

4.5.1. Comparison with Mars

Two craters in the southern highlands, that have already been studied, have been chosen as reference for our comparison (Fig. 1). Bakhuysen crater (15.39°E, 23.9°S) has 35 valley networks mapped by Hynek et al. (2010) and are interpreted as fluvial valleys by Moore (2005) (Fig. 5). A crater, refered as "GLF-crater" in this study (28°16'E, 31°58'S), defined by Souness and Hubbard (2012) as a crater with Amazonian GLFs (Fig. 6). We supposed that the valleys in this crater were mainly shaped by the GLFs present in this crater. We applied our method to the valleys in these craters. The results thus obtained allowed us to verify if our method is consistent with the interpreted origin of the valleys (Moore, 2005; Hynek et al., 2010; Souness and Hubbard, 2012). Moreover, with the data obtained, we were able to build a database large enough to compare these known cases with the valleys in our study areas.

4.5.2. Comparison with the Earth

In order to compare the martian results for the valleys, we decided to apply the method described above (Section 4.3) in the area of Chamonix in the French Alps (Fig. 7). This terrestrial glacial landscape present several glaciated valleys and contrary to our study area, the glacial valleys in Chamonix still have their glacier (Mer de Glace, Argentière glacier...; Zemp et al. 2011; Frezzotti and Orombelli 2013). Then some measured parameters such as the depth and the cross-sectional are distorted, they should increase without the glacier.

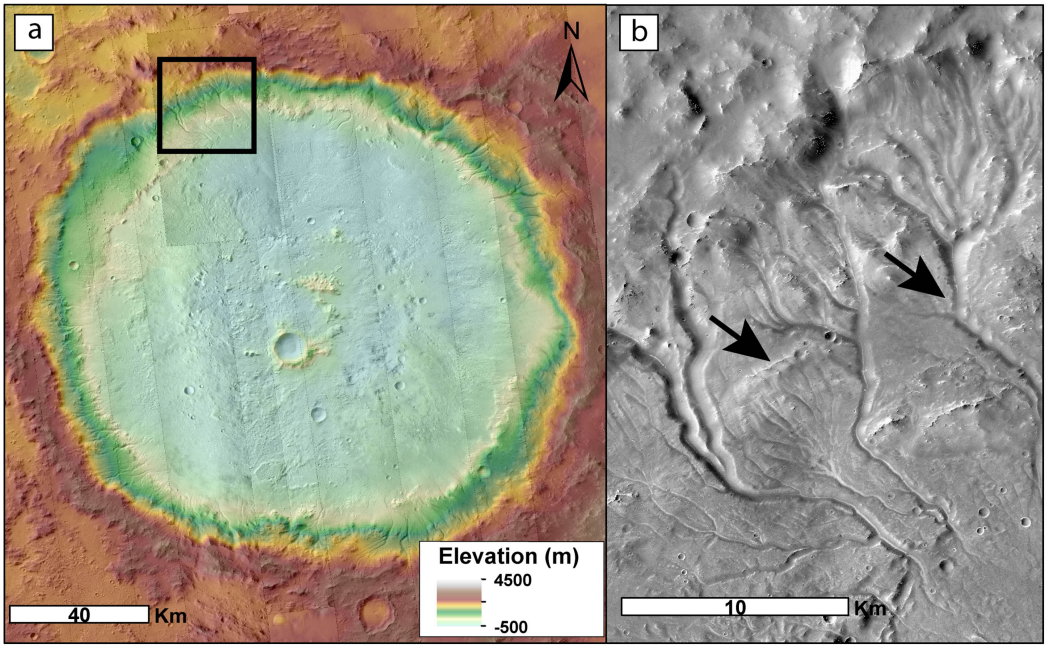

Fig. 5. Bakhuysen crater (a) Background using CTX images (G05_020309_1568_XN_23S343W; G12_022933_1578_XI_22S344W; B18_016551_1566_XN_23S344W; B20_017263_1573_XI_22S343W; B18_016617_1562_XI_23S345W; B17_016195_1563_XN_23S345W; P11_005475_1569_XN_23S343W) and MOLA elevation data. (b) Detailed view of the fluvial valleys shown in (a) (G12_022933_1578_XI_22S344W). Images credit NASA/JPL/University of Arizona.

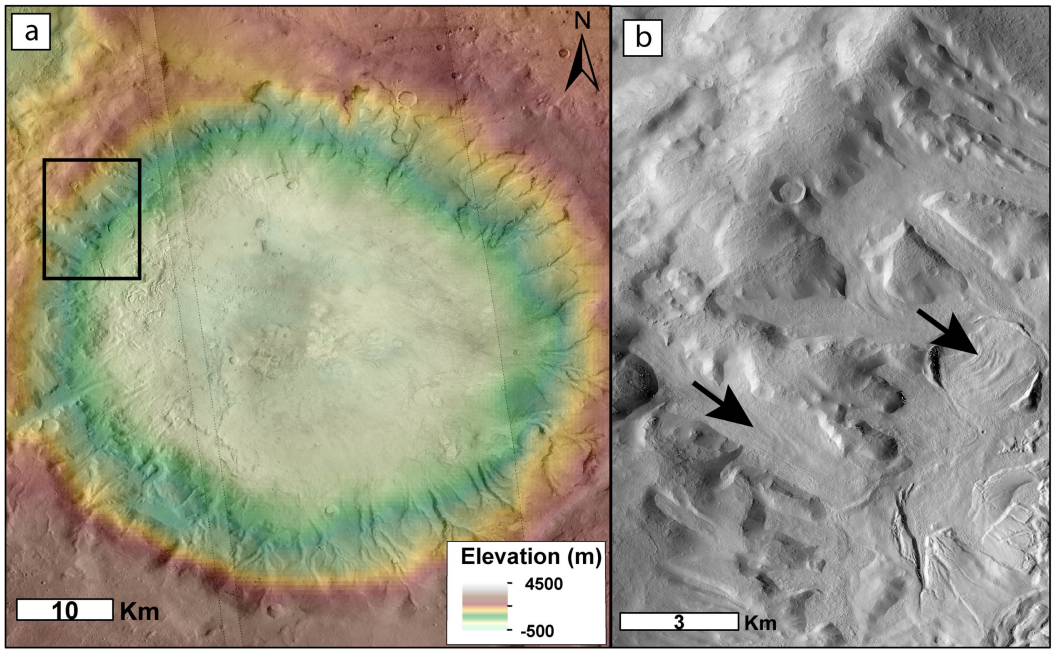

Fig. 6. GLF-crater (a) Background using CTX images (P07_003589_1466_XN_33S331W; B11_013966_1476_XN_32S331W; B06_011909_1480_XN_32S332W) and MOLA elevation data. (b) Detailed view of the valleys and GLF shown in (a) (B06_011909_1480_XN_32S332W). Images credit NASA/JPL/University of Arizona.

However, the other parameters are measurable even if a glacier is present. Indeed, the current presence of a glacier does not influence the length and the width of the valleys because the main glacial erosion phase is over since the Holocene which correspond to the maximum glacier extent (Zemp et al., 2011).

4.6. Summary of measured parameters

4.6.1. Valleys in Terra Sabaea

Using our morphometric analysis we characterized 140 valleys with different origins, namely 36 fluvial valleys in Bakhuysen crater (Moore, 2005; Hynek et al., 2010), 23 glacial valleys in GLF-crater (Souness and Hubbard, 2012) and a suite of valleys with unknown origin: 42 from Dawes crater, 33 from Crater 1 and 6 from mountain 1. We constructed a database with more than 2500 usable measurements to determine whether the valleys of Dawes crater, Crater 1 and mountain 1 are fluvial or glacial in origin. We plotted frequency distributions for each measured parameters (Fig. 8a-d). The average value for each studied parameter is presented in Table 10 in the supplementary. Hynek et al. (2010) identified 35 fluvial valleys in Bakhuysen crater and 29 fluvial valleys in Dawes crater. We re-examined these valleys using more morphometric parameters and we added new valleys to this dataset (Fig. 9).

4.6.2. Valley heads in Terra Sabaea

We identified 100 valley heads in the study area, namely 75 valley heads in Dawes crater and 25 in Crater 1. We plotted frequency distributions for each measured parameters (Fig. 10a-f). The average value for each of the studied parameters is presented in Table 11 in the supplementary. We did not find any valley heads in mountain 1. We constructed a database, with more than 700 usable measurements, to characterise these valley heads and to compare them with terrestrial morphologies (Fig. 11).

4.6.3. Glacial valleys in Chamonix valley

We identified 13 glacial valleys in Chamonix valley. The values for each studied parameter is presented in Table 9 in the supplementary. We constructed a database, with more than 250 measurements, usable as terrestrial reference from our method. The tables containing all the measured parameters for each area are in the supplementary material (Table 4-9).

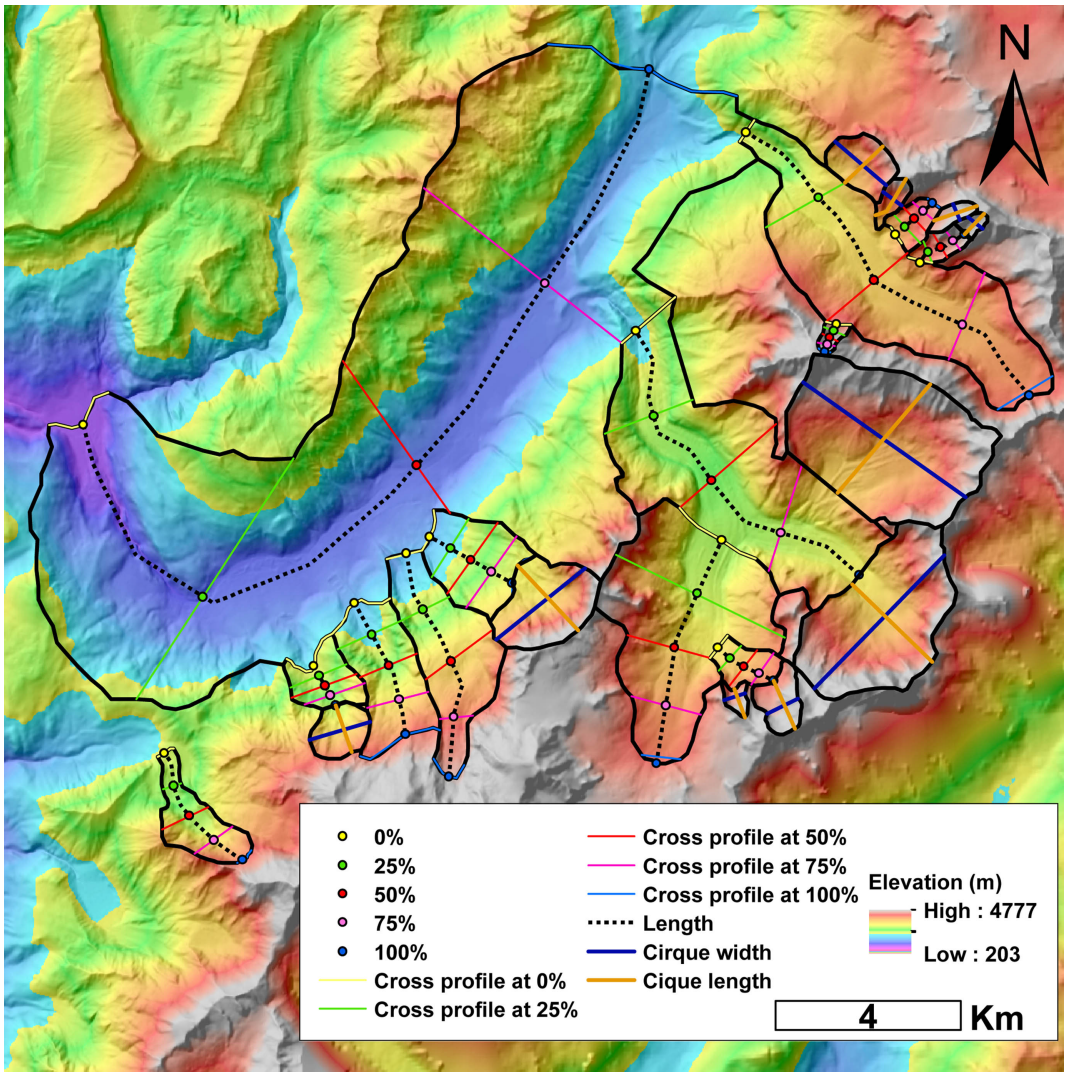

Fig. 7. Study area of Chamonix in the French Alps on Earth. Colorized elevation data from 25m/pixel DEM BDALTIr_2-0_ASC_25M_LAMB93_IGN69_D073. Images credit IGN-F

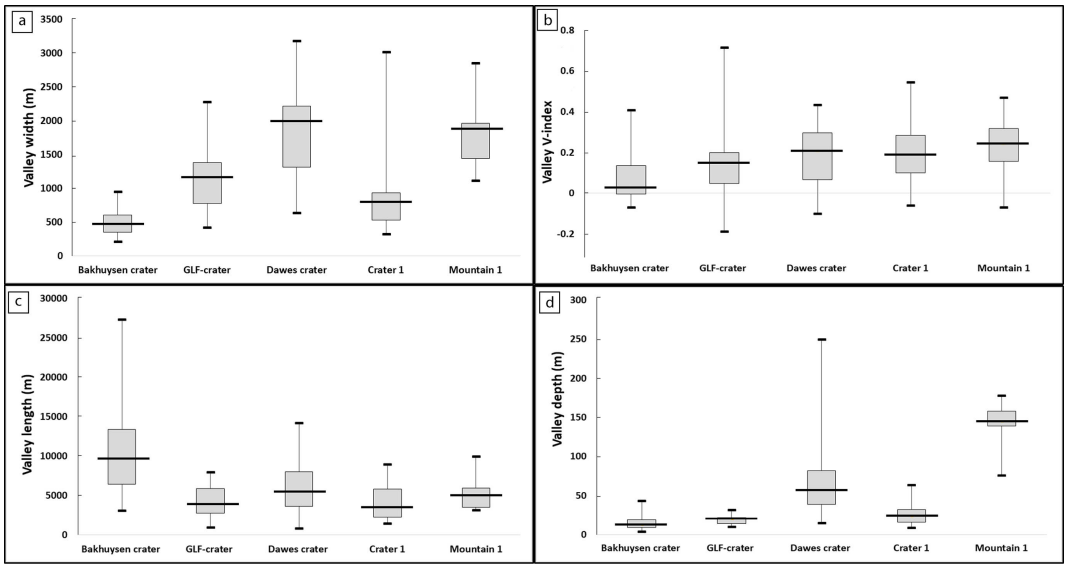

Fig. 8. Box and whisker plot of valley (a) width, (b) V-index, (c) length and (d) depth. The short black lines represents the maximum and minimum for each dataset. The box represent the interquartile range, with Q1 and Q3 the bottom and top of the box.The median is represented by the long black lines in the boxes.

4.7. Age estimation of Dawes crater

In order to constrain the age of the valleys, we performed a crater size-frequency analysis, or "crater counting". We measured the crater size-frequency distribution (the number and size of craters accumulated on surface units) using CTX images to estimate the age for Dawes crater (Hartmann and Neukum, 2001; Ivanov, 2001). We observed that the floor of Dawes crater is covered by materials that partially overlaps the base of the crater wall. This deposit partially covers the valleys showing that this material was deposited after valley formation. Hence, the valleys and valley heads are younger than the crater walls but older than the filling material that covers them. Therefore, estimating the age of the crater floor and the craters inner walls allowed us to bracket the maximum and minimum age of the valleys and valley heads. We defined two count areas, the first one is the crater inner walls delimited by the crater rim and the break in slope with the crater floor. This area is characterized by the presence of valleys and valleys heads. The second is the crater floor characterized by a flat floor, strongly cratered and the complete absence of valleys and valley heads. We measured all impact craters $>$ 1 km, except secondary and ghost crater using CraterTools in ArcGIS (Kneissl et al., 2011) in these two areas. Dawes crater has 96 superposed craters $>$ 1 km over an area of 28439 m^2. The crater size-frequency distributions was plotted with Craterstats 2.1 software using a cumulative plot and using the function chronology from Hartmann and Neukum (2001) and Hartmann (2005). The crater

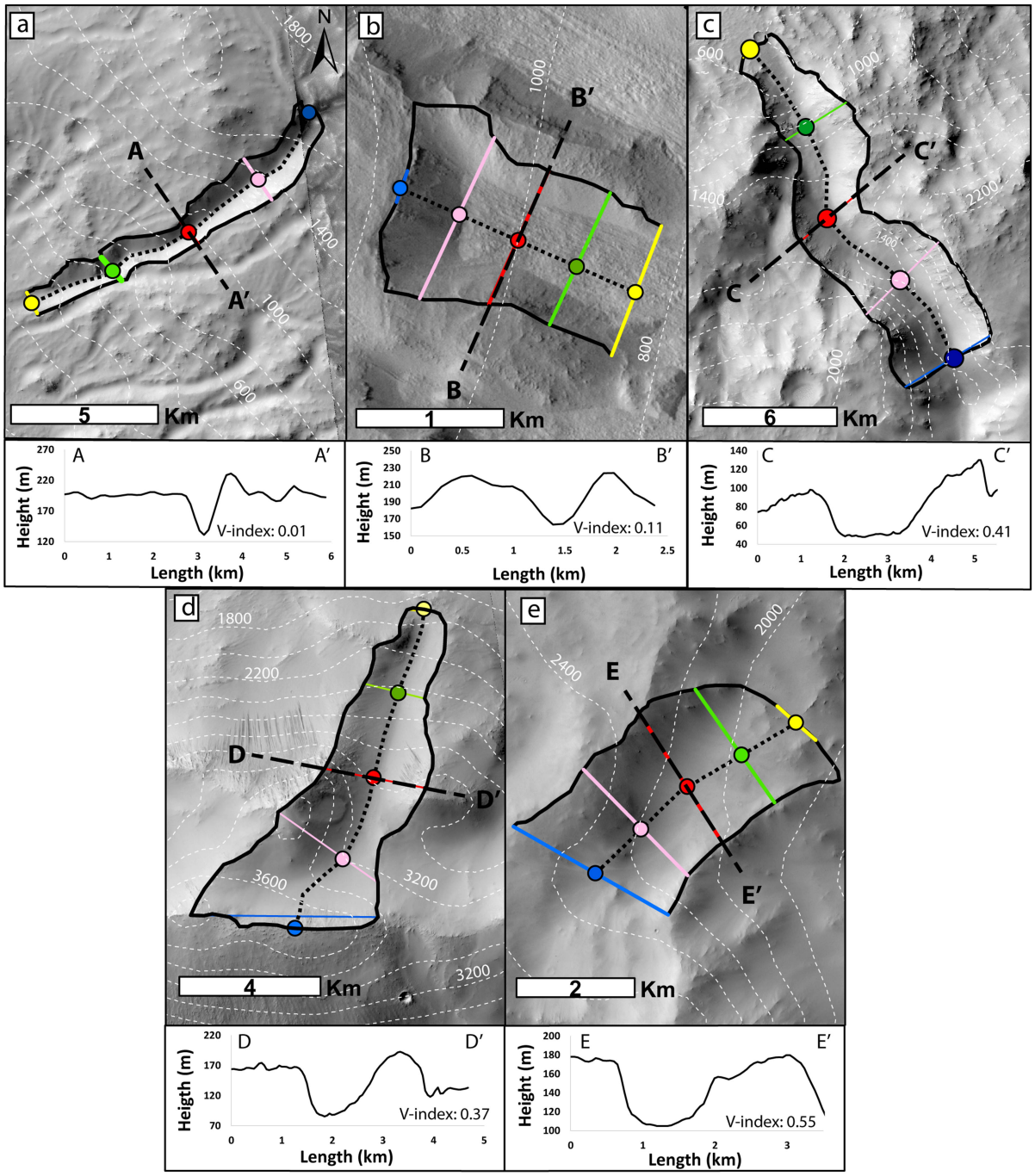

Fig. 9. Example of studied valleys and their associated V-index. The dashed line shows the cross-section at 50% of the downstream valley length extract from HRSC elevation data. Valley examples from (a) Bakhuysen crater (CTX: B20_017263_1573_XI_22S343W), (b) GLF-crater (CTX: B06_011909_1480_XN_32S332W), (c) Dawes crater (CTX: B01_010102_1699_XN_10S321W), (d) mountain 1 (CTX: G19_025833_1759_XN_04S317W), (e) Crater 1 (CTX: G02_019174_1705_XN_09S318W). The legend is the same as Fig. 4a. Images credit NASA/JPL/University of Arizona.

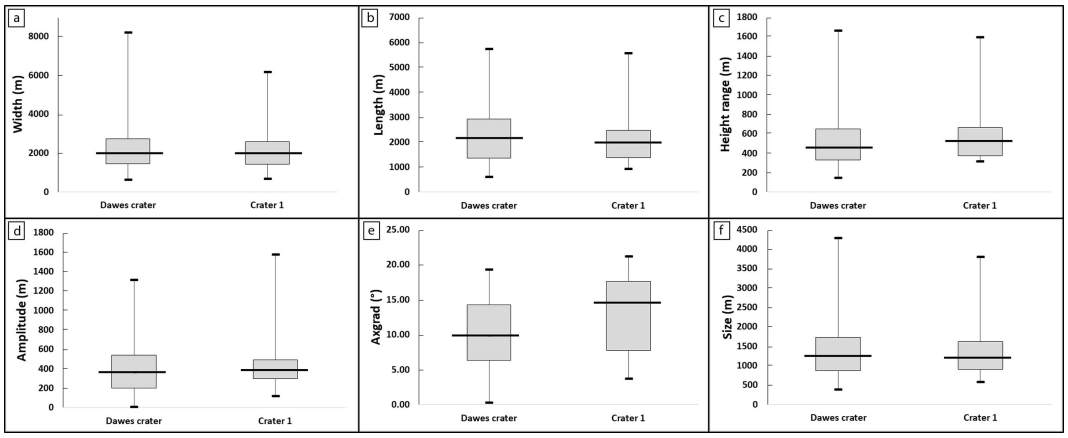

Fig. 10. Box and whisker plot of valley head: (a) width, (b) length, (c) altitudinal range, (d) amplitude, (e) axial gradient and (f) size.

size-frequency distribution is not significative for crater 1, in fact, the plot obtained does not fit with any of the established crater density boundaries (Tanaka, 1986; Hartmann, 2005). However, in order to constrain the age of the valley in crater 1, we counted the craters with diameter $>$ 1 km and calculated the N(1) to determine the formation period of the valleys using established crater density boundaries (Bouley. and Craddock, 2014). N(1) is the density of craters with a diameter $>$ 1 km normalized to an area of $10^6 km^2$. This method was realized in two count areas in crater 1, the floor and the crater inner walls defined as the same way described above. We also applied the "N(1) method" to Dawes crater in order to check if the two ages found with the different methods are consistent. Mountain 1 only have 3 craters $>$ 1 km it is not enough to realize a significative crater size-frequency analysis.

5. Results

5.1. Morphometric comparison: Valleys

5.1.1. Length to Width ratio

The valleys from Dawes crater, Crater 1, mountain 1, and GLF-crater have a mean length to width ratio of 2.5, being only slightly longer than they are wide (Fig. 12). The Bakhuysen valleys are significantly longer compared to their width, with a mean length to widtht ratio of 22 (Fig. 12). The difference between the length to width ratio suggests that the formation process was not the same for Bakhuysen crater as for the

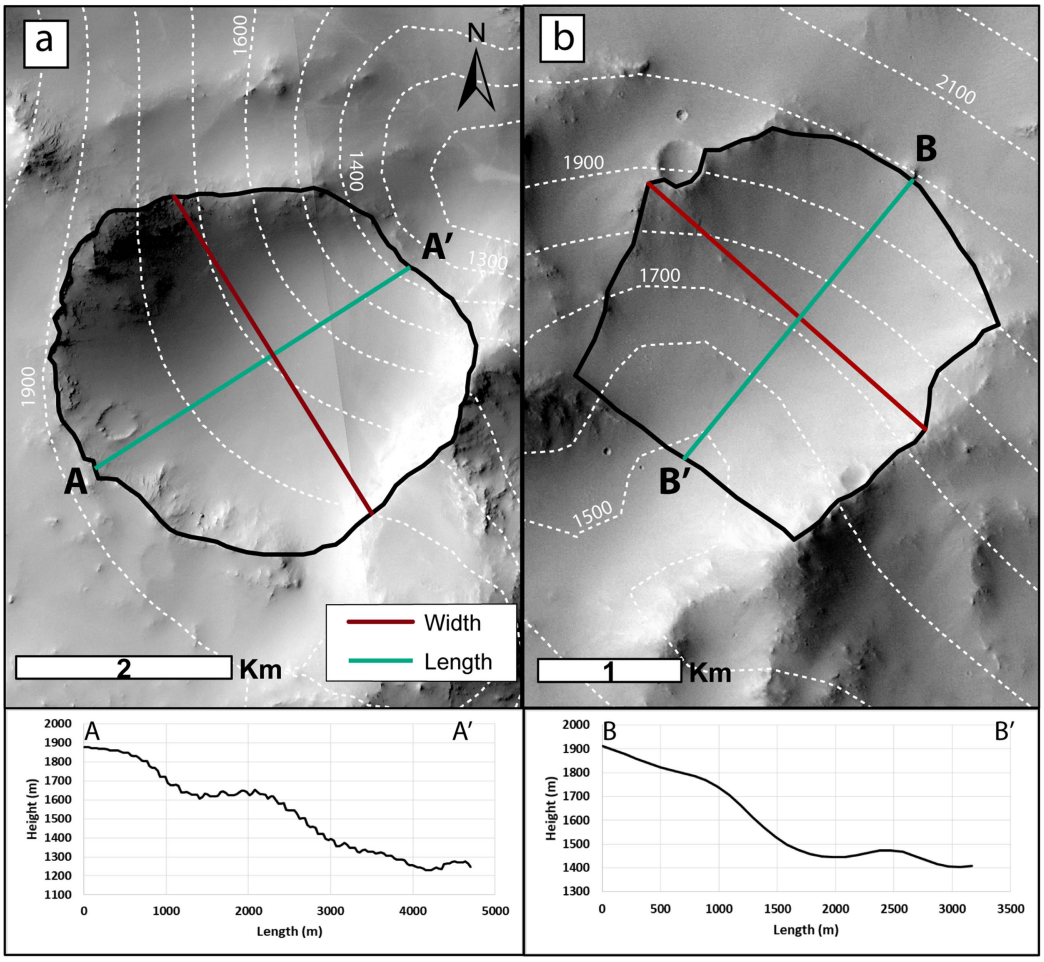

Fig. 11. Example of studied valley heads. The length line shows the location of the longitudinal cross section included underneath each image. Valley head from (a) Dawes crater southeast inner rim (CTX B19_017104_1709_XN_09S323W) (b) Crater 1 northwest inner rim (CTX: B16_015917_1710_XN_09S317W). Images credit NASA/JPL/University of Arizona.

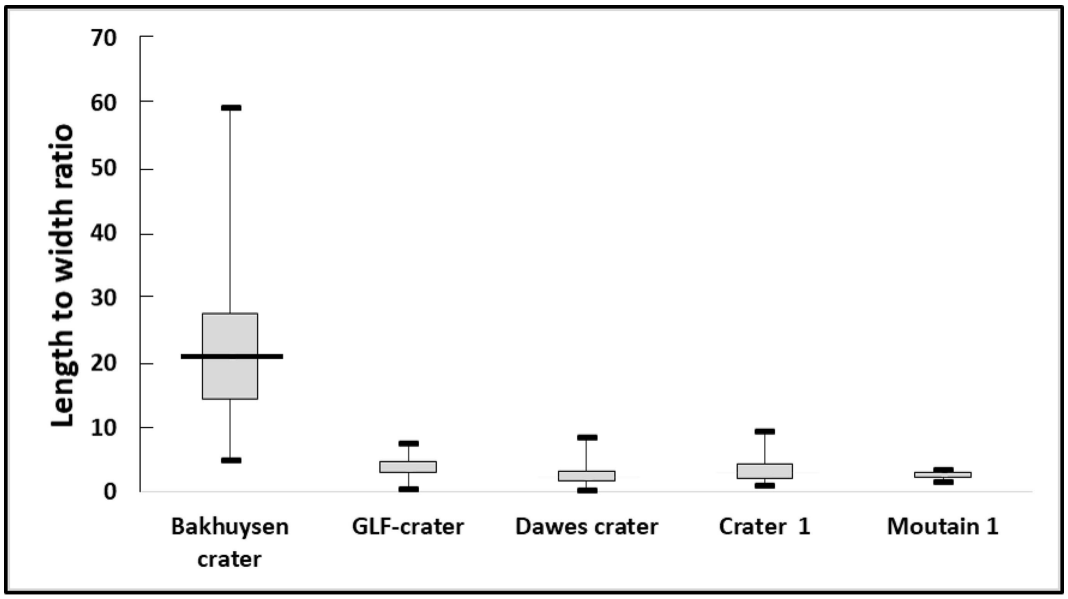

Fig. 12. Box and whisker plot of length to width ratio for valleys in each study areas. 140 valleys have been plotted, 36 from Bakhuysen crater, 23 from GLF-crater, 42 from Dawes crater 33 from crater 1 and 6 from mountain 1 . The median values are respectively: 20.8; 3.6; 2.3; 2.8 and 2.7.

other valleys. Long and narrow valleys are formed by fluvial processes and have an aspect ratio $>>1$ while short stubby valleys are generally formed by glacial erosion with an aspect ratio >1 (Hobbs et al., 2016). Thus, our analysis supports the fluvial interpretation for the Bakhuysen valleys and suggests the origin of the valleys from GLF-crater, Dawes crater, Crater 1, and mountain 1 are different.

5.1.2. Cross-sectional area

Based on our analysis of the valley ratio cross-sectional area/ drainage area we can distinguish two groups (Fig. 13a). The first one is composed of Bakhuysen crater valleys, the ratio between the cross-sectional area and the drainage area is low with an average value of 0.001. The second group is composed of Dawes crater, Crater 1, mountain 1, and GLF-crater, the ratio between the cross sectional area and the drainage area is higher than for Bakhuysen. The average values is about 0.004, that is four times higher than Bakhuysen one (Fig. 13a). On Earth, this value of four is the characteristic difference between the glacial and fluvial valleys (Montgomery, 2002). Moreover, the cross-sectional profiles reveal that Bakhuysen valleys have a V-shape characteristic of a fluvial erosion (Penck, 1905; Roberts and Rood, 1984; Livers and Wohl, 2015) and that Dawes crater, Crater 1, mountain 1, and GLF-crater valleys have a U-shape which is characteristic of a

glacial erosion (Fig. 9). In order to confirm this result, we realized a statistical test to verify if the data are statiscally different. The five populations are not normally distributed so we chose to use the Mann-Whitney U test. This method is used to test whether two samples are likely to derive from the same population. This nonparametric test is applicable when the samples are small (N<40), not normally distributed and independent which is the case for this study. To achieved this, the first step was to rank the cross-sectionnal area/drainage area values to obtain the critical value of U and compare it with the values in Mann-Whitney table for a given N (Table 12 in supplementary). To give an example, let compare the two populations of valleys from Bakhuysen crater (N = 35) and Moutain 1 (N=6). After ranking, we obtained a critical U value of 6. For these populations, the U value in the table is 37. The critical U value from our data is strictly inferior than the U given in the Mann-Whitney table. So we can confirm that the valleys from Bakhuysen crater and Mountain 1 are statiscally separated, that mean that the cross-sectionnal area/drainage area for these two population of valley do not follow the same trend. In other words, the erosion processes between these two populations of valleys are not the same. We applied this test to the other populations and we found the same result.

The Fig. 13b shows the variation of the cross-sectionnal areas all along the valleys in the differents areas. From the top of the valley (100%) down to the middle of the valley (50%) the cross-sectionnal area increases and then decreases downstream to the end of the valley (0%). This variation follows the law of ajusted cross section described by Penck (1905) for the alpine glacial valleys on Earth.

5.1.3. Elevation

Based on the elevation of the valleys, we can distinguish two groups. The first, comprises valleys in Bakhuysen crater, are found at an elevation <1000 m, 168 m on average (Fig. 14). The second group is made up of valleys from GLF-crater, Dawes crater, Crater 1 and mountain 1, where 95% the valleys are located at an elevation higher than 1000 m with an average of 1722 m (Fig. 14). These valleys are at an elevation 10 times higher than the valleys in Bakhuysen crater. On Earth, the elevation of glacial valleys is higher than fluvial ones (Roberts and Rood, 1984; Montgomery, 2002). .

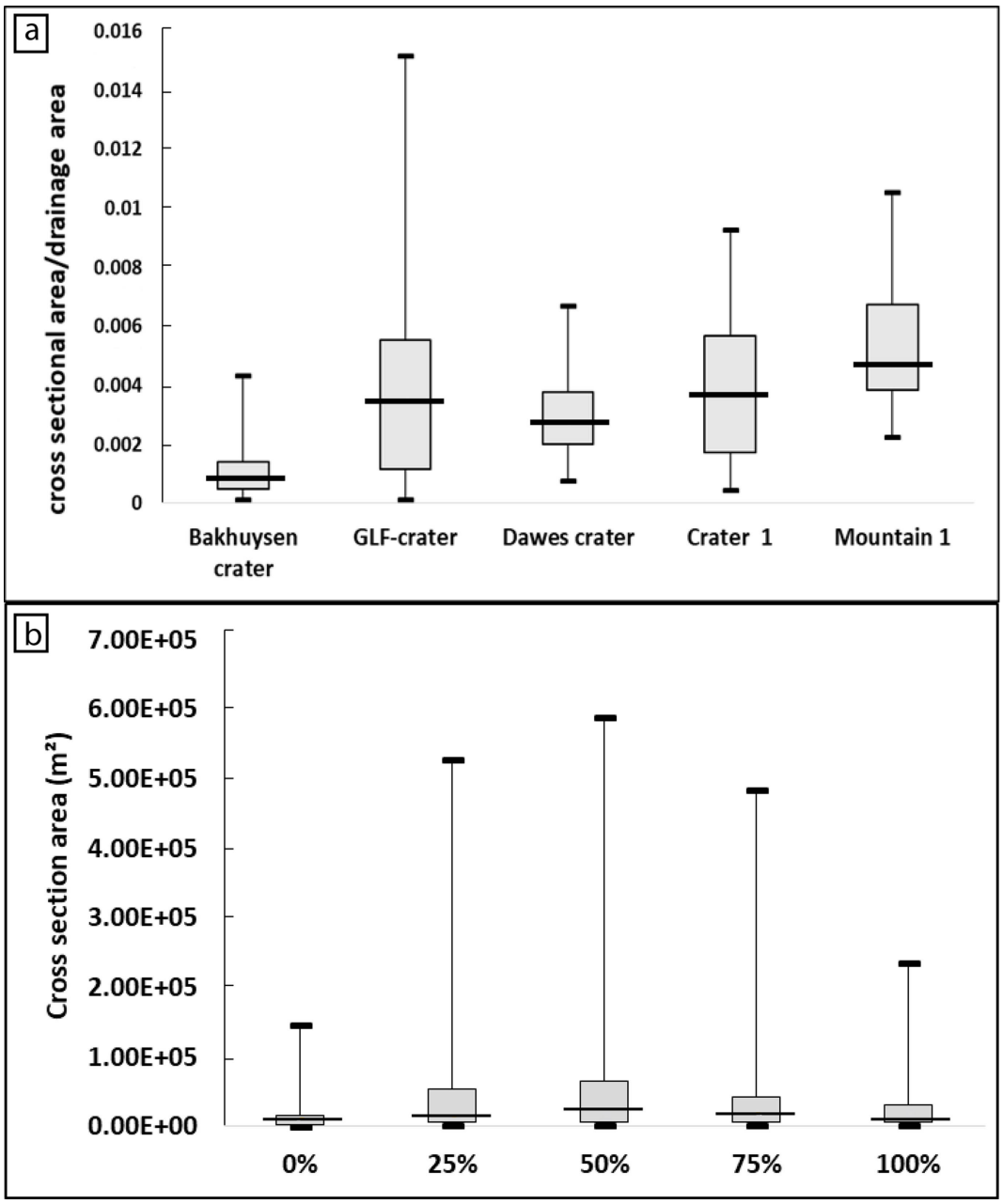

Fig. 13. (a) Box and whisker plot of cross-sectional area/ drainage area for the studied valleys. We can observe two groups, one composed of the valley from Bakhuysen crater with a mean cross sectional area/drainage area of 0.001 and the second composed of GLF-crater, Dawes crater, Crater 1, and mountain 1 with a mean cross sectional area/drainage area of 0.004. (b) Box and whisker plot of cross-section area at 0%, 25%, 50%, 75% and 100% of the valley length for Dawes crater, Crater 1 and Mountain 1.

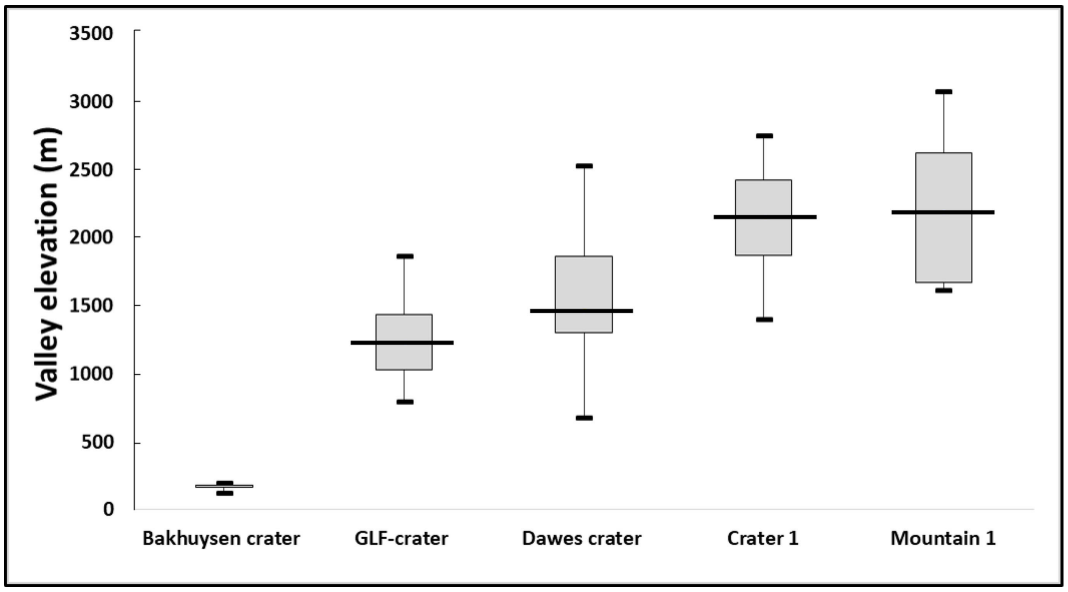

Fig. 14. Box and whisker plot of elevation of the identified valleys from MOLA elevation data.

5.2. Morphometric comparison: valley heads

The valley heads in Dawes crater and Crater 1 have a sizes ranging from 372 m to 4282 m (Fig. 10 f). Furthermore, the longitudinal profile shows a steep upstream slope, between 26° to 28°, and a gentle downstream slope between 17° to 20° (Fig. 15 a-b). On the 75 valley heads identified in Dawes crater 32 presents a topographical lip and 43 do not. For Crater 1, 13 valleys heads have a topographical lip on 25 measured valley heads. These topographical lips have a height between 20 and 100 m (Fig. 15a-b). The average value for each compared parameters is presented in Table 11 in the supplementary.

5.3. Morphometric comparison: glacial valleys in Chamonix

In order to compare the measurement made on Mars with known case on Earth, we plotted length against width for each valley in our study areas and compared them with the results we obtained on 13 glacial valleys in Chamonix (Fig. 16). This plot reveals two groups, the first, comprises valleys in Bakhuysen crater that are longer than wider (Section 5.1.1). The second comprises valleys in Dawes crater, Crater 1, GLF-crater, moutain 1. The point here is that valleys from the second group follow the same trend than Chamonix ones. The V-index is also comparable, in fact Dawes crater, Crater 1 and moutain 1 have a mean V-index of 0.20, 0.21, 0.23 respectively and the glacial valleys from Chamonix have a mean V-index of 0.21. Moreover, the mean length to width ratio is 3.21 (Table 10 in the supplementary). These results suggest that the

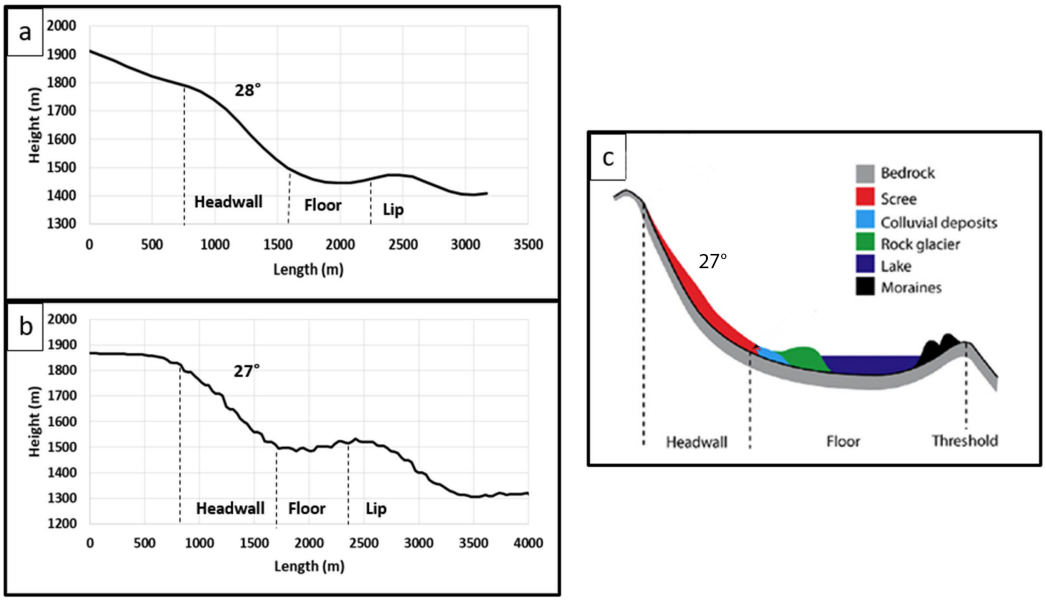

Fig. 15. Longitudinal profile of valley heads from HRSC DTMRDR. (a) In Dawes crater (h5184_0000_da4), (b) In Crater 1 (h1961_0000_bl3), (c) Longitudinal profile of a typical terrestrial glacial cirque. Modify from Barr and Spagnolo (2015)

valleys from Dawes crater, Crater 1 and moutain 1 are eroded by the same processes than glacial valleys from Chamonix.

6. An interpreted glacial landscape in Terra Sabaea

6.1. Characteristics of glacial valleys in Terra Sabaea

The measured parameters of the valleys in Dawes crater, Crater 1, and on mountain 1 are similar to terrestrial glacial valleys:

1. Dawes crater, Crater 1 and mountain 1 valleys have a length to width ratio >1, which more similar to the GLF-crater valleys than to Bakhuysen fluvial valley which have a length to width ratio >>1 (Fig. 12b)
2. Dawes crater, Crater 1 and mountain 1 valleys have a cross-sectional areas that are four times larger than Bakhuysen fluvial valleys and a similar cross-sectional area to the GLF-crater valleys (Fig. 13a)

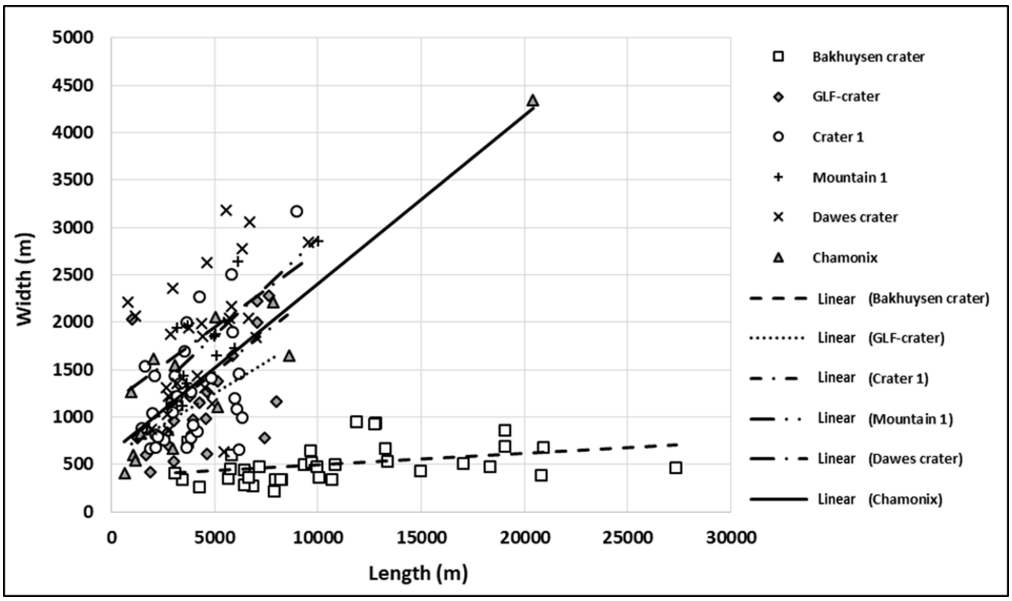

Fig. 16. Length versus width for all the valleys from the different study areas.

3. Dawes crater, Crater 1 and mountain 1 valleys have a V-index around 0.20 while Bakhuysen fluvial valleys have a V-index around 0.07 (Fig. 8b)
4. Dawes crater, Crater 1 and mountain 1 valleys have an elevation 10 time higher than Bakhuysen and a similar elevation to GLF-crater valleys (Fig. 14)
5. Dawes crater, Crater 1 and mountain 1 valleys have a U-shape while Bakhuysen morphologies have a V-shape (Fig. 9c-e)
6. Dawes crater, Crater 1 and mountain 1 valleys respect the cross-section law characteristic of terrestrial glacial valleys (Fig. 13b)

6.2. Characteristics of valley heads in Terra Sabaea

The longitudinal profiles of valley heads in Dawes crater and Crater 1 are similar to typical longitudinal profiles of glacial cirques on Earth (Fig. 15c). They have a steep upstream slope of about 28° in the headwall, then a gentle downstream slope about 20° on the floor, with a topographic lip marking the end of the feature (Fig. 15). The other measured parameters, reported in Fig. 10 and in Table 11 in the supplementary, are within the range of the highest terrestrial glacial cirques measured (Barr and Spagnolo, 2015; Evans and Cox, 2017). The mean axial gradient measured is low, 9.97° in Dawes crater valley heads and 13.18° in Crater

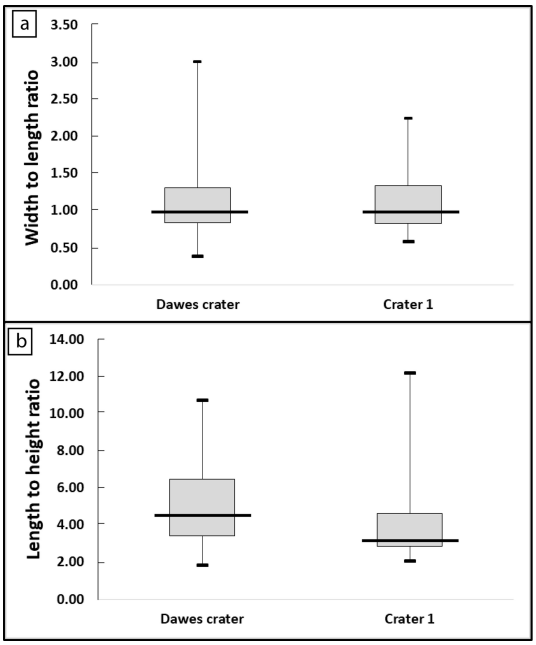

Fig. 17. Box and whisker plot of (a) valley head width to length ratio, (b) valley head length to height ratio.

1 valley heads (Fig. 10e) compared to the mean axial gradient measured on Earth but still in the range of terrestrial glacial cirque (Barr and Spagnolo, 2015; Evans and Cox, 2017). The width to length ratio is around one, which correspond to terrestrial glacial cirque (Fig. 17a) and the length to height ratio is in the range of terrestrial glacial cirques measured on Earth by Barr and Spagnolo (2015) and Evans and Cox (2017; Fig. 17b).

The morphological and geometrical similarities of the valley heads and the valleys to terrestrial glacial cirques and valleys, strongly suggests that the origin of the valleys in Dawes crater, Crater 1 and on mountain 1 is glacial. Moreover, the fact that the valleys in Dawes crater and Crater 1 are also associated with features strongly resembling glacial cirques strengthens the interpretation that Dawes crater and Crater 1 exhibit relict glacial landscapes (Fig. 18a-f).

6.3. Timing of the formation of the glacial landscape

In order to constrain the potential age of the glacial landscape, undertook an analysis of the crater-size frequency distribution for Dawes crater. The crater size-frequency distribution for the floor of Dawes crater gives a best-fit age of 3.52 $\pm$ 0.05 Ga and 3.66 $\pm$ 0.03 Ga for the inner wall with Hartmann and Neukum (2001) chronology function (Fig. 19a). With Hartmann (2005) chronology function, the best-fit age is 3.34

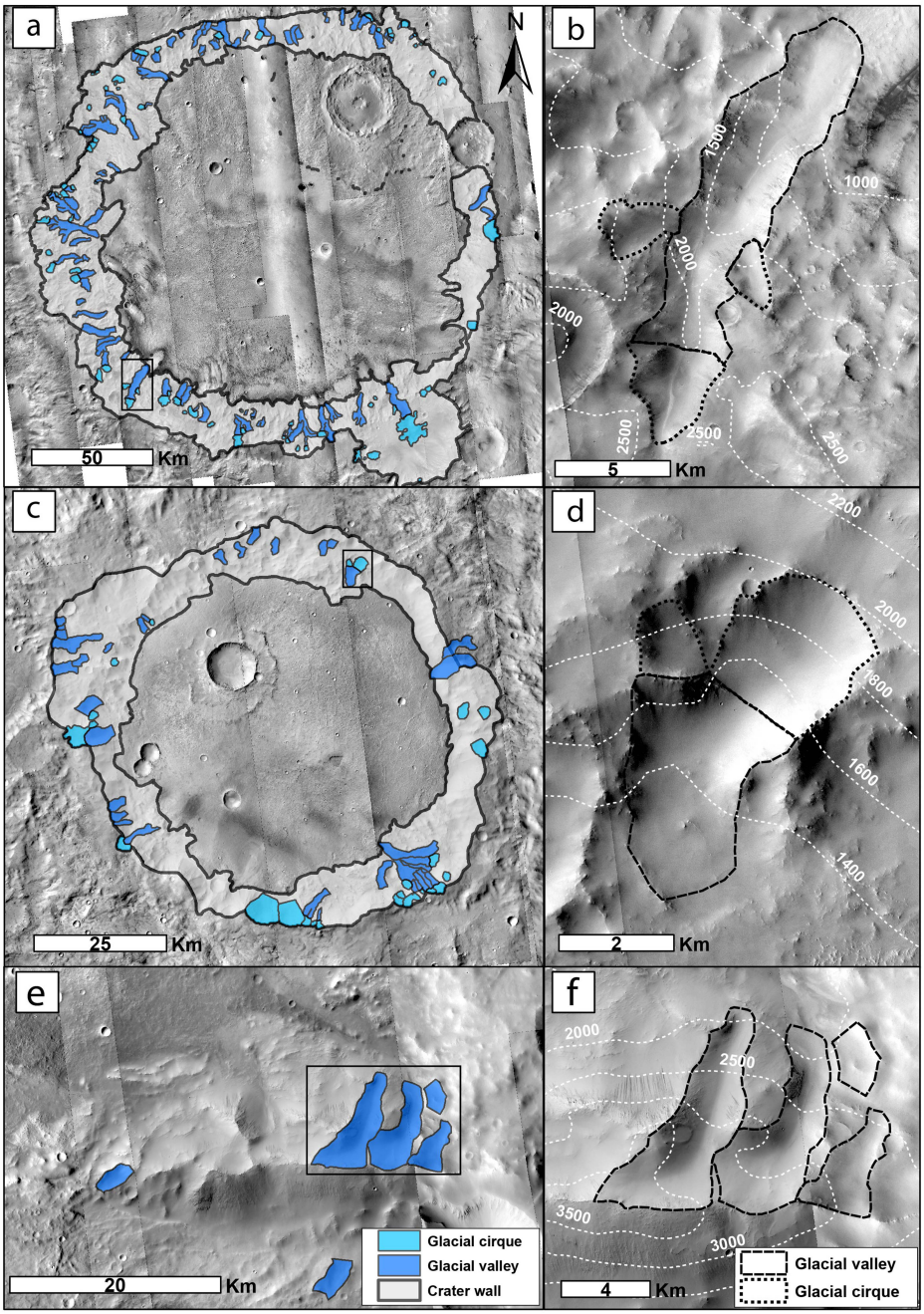

Fig. 18. Geomorphological map of the proposed glacial landscape. (a) Dawes crater distribution of the glacial valleys and cirques on the inner wall of the crater overlain on CTX images. (b) Detail of glacial assemblage, the main glacial valley is surrounded by three glacial cirques. (c) Crater 1 distribution of the glacial valleys and cirques on the inner wall of the crater overlain on CTX images. (d) Detail of glacial assemblage, the main glacial valley is surrounded by two glacial cirques. (e) Mountain 1 distribution of the glacial valleys on the wall of the moutain overlain on CTX images. (f) Detail of glacial valleys, we can not found glacial cirque on that mountain. Images credit NASA/JPL/University of Arizona.

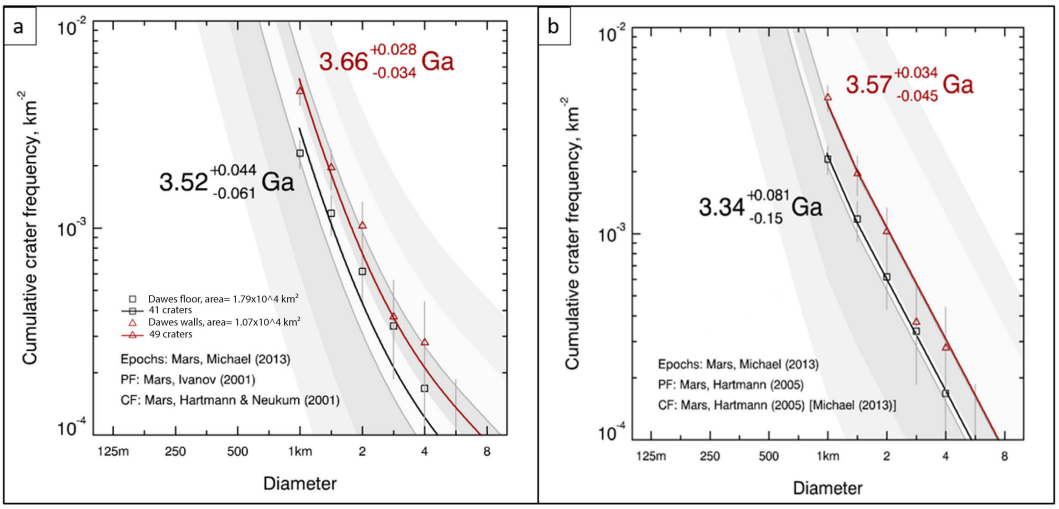

Fig. 19. Timing of formation of the glacial landscape in Dawes crater. (a) Results are for crater with diameter > 1 km with Hartmann and Neukum (2001) chronology function. The red triangles represent the counts performed on the inner wall (3.66 Ga) and the black squares the counts performed on the crater floor (3.52 Ga). (b) Results are for crater with diameter > 1 km with Hartmann (2005) chronology function. The red triangles represent the counts performed on the inner wall (3.57 Ga) and the black squares the counts performed on the crater floor (3.34 Ga). A detail map of the count area is in the supplementary (Fig. 21).

± 0.06 Ga for the floor, and 3.57 ± 0.03 Ga for the inner wall (Fig. 19b). So the age of the Dawes crater glacial landscape is probably between 3.34 and 3.66 Ga (Late Noachian/ Early Hesperian).

Dawes crater has N(1) = 4579 for the walls and N(1) = 2291 for the floor. We applied this method to Crater 1 and we found N(1) = 4167 for the walls and N(1) = 3297 for the floor. In the two craters, the crater densities correspond to the Late Noachian/Early Hesperian for the inner walls and to the Hesperian for the floor according to the established crater density boundaries (Tanaka, 1986; Hartmann, 2005). These ages are consistent with the age found by Bouley. and Craddock (2014) with the basin age-dating method for the basins and subbasins within Terra Sabaea of 3.61 ± 0.02 Ga. So, we hypothesize that from the Late Noachian to the Early Hesperian, the climate was cold enough to have deposition and preservation of ice leading to formation of glaciers and for the crater walls to be shaped by ice processes and form a glacial landscape.

7. Discussion

7.1. Allometry and origin of the glacial cirque in Terra Sabaea

The glacial cirque distribution in Dawes crater and Crater 1 shows that some of them are located at lower elevations than some glacial valleys. On Earth, glacial cirques are usually at higher elevations than the

downstream glacial valleys. The sizes and allometric coefficients of the cirques provides information which can explain the differences in the topographic characteristic of cirques on Mars compared to the Earth. Cirque size is calculated in order to assess whether cirques have developed isometrically or allometrically and it is plotted against the length, width and altitudinal range (Barr and Spagnolo, 2015). The allometric coefficients of logarithmic regressions indicate if the cirque growth equaly in the three dimensions (isometric) or unequaly (allometric), when the allometric coefficients are close to 1 the cirque population displays isometric properties and when they are significantly different from 1 the cirque population displays allometric properties. The sum of these coefficients must be 3 (Evans, 2010; Barr and Spagnolo, 2015; Delmas et al., 2015). The allometric coefficients for all the three dimension are close to 1 in Dawes crater and Crater 1 and they sum to 3 (Fig. 20a-b). So the glacial cirques identified in Dawes crater and Crater 1 are isometric. The apparent isometry of cirque indicate that former glacier rarely extended beyond their cirques because a glacier confined to its cirque may naturally result in isometric developement, but, on Earth, glaciers often grow beyond cirque confines and shape glacial valley downstream (Barr and Spagnolo, 2015). In our study, we found both, cirques connected and unconnected to a glacial valley. Delmas et al. (2015) proposed that the isometric character of cirques could be interpreted as a process by which nonglacial topographic depressions with allometric properties were progressively shaped by ice to form isometric landforms. We proposed that on Mars, this nonglacial topographic depressions could be a pre-existant impact crater filled later by the ice. This hypothesis could explain (1) the isolated cirques which are not linked with a glacial valley and (2) the fact that some glacial cirques are found at lower elevations than glacial valleys. Moreover, if some of glacial cirques have an impact crater as origin, the impact crater diameter should be >2 km (Fig. 10a-b, Table 11). These craters later filled by the ice became glacial cirques with high size. So this hypothesis can also explain (3) the fact that the measured parameters are high but within the range of the highest terrestrial glacial cirques.

7.2. Type of glaciation

On Earth, cold-based glaciers have temperatures below the pressure-melting point at near their base (Nagle and Witherick, 2002; Cogley et al., 2010). Their movement is a result of internal plastic deformation inside the ice, and only little, if any, basal abrasion occurs. Warm-based glaciers have at their base temperatures at pressure melting points, they melt from their bed, resulting in basal sliding in which a water film lubricates the surface. Extensive basal abrasion occurs (Hargitai and Kereszturi, 2015). These differences of erosion involve that glacial depositional features such as moraines, kames, eskers, or kettles hole are generally typical

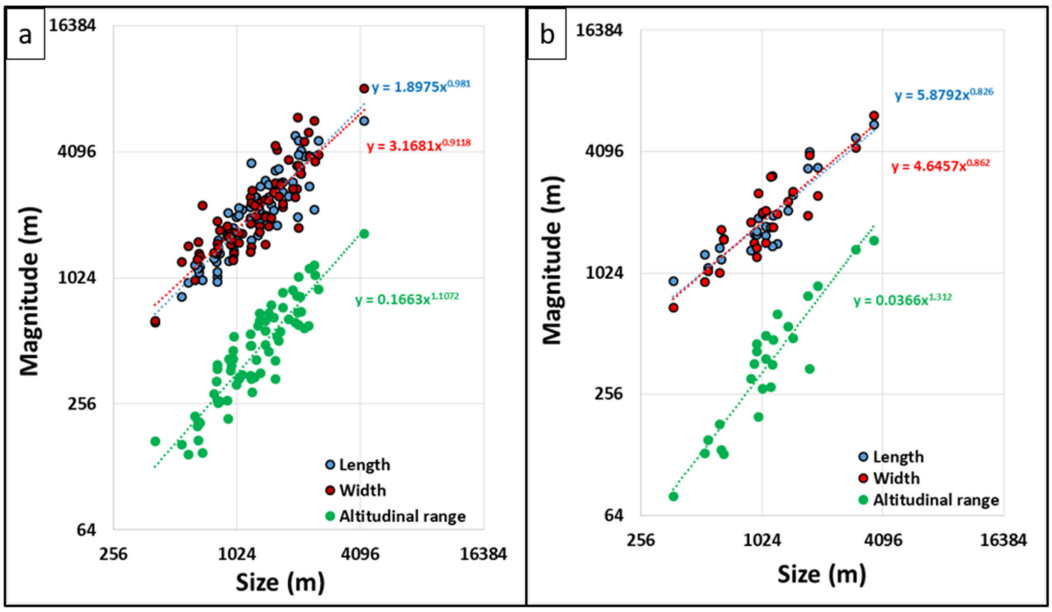

Fig. 20. Valley head morphometry. (a) Allometric (double log (4)) plot of valley heads from Dawes crater (N=77). the allometric coefficients are 0.98 (length), 0.91 (width) and 1.1 (altitudinal range). (b) Allometric (double log (4)) plot of valley heads from Crater 1 (N=25) the allometric coefficients are 0.82 (length), 0.86 (width) and 1.3 (altitudinal range). The size is calculated from $\sqrt[3]{LWH}$ and the magnitude is the differents values from the length, width and altitudinal range.

of warm-based glacier. In Terra Sabaea, the glacial valleys do not have any of these features. This absence could be because these depositional features are composed of easily erodable unconsolidated sediment, and have been removed by subsequent erosional episodes like, erosion by wind, meteoritics impacts or run-off. When a glacier melts, a large amount of liquid water flows down the slope. We propose that the water thus liberated could have eroded and transported away these characteristic depositional features. Therefore, it is difficult to infer if the glaciers that created these valleys were warm or cold based. However, the morphometric properties highlighted in this study allow us to differentiate between the types of glaciation responsible for there valleys (alpine glacier or ice cap). Our morphological and geometrical results are consistent with terrestrial alpine glaciers as defined by Jackson et al. (2005) as any glacier in a mountain range except an ice cap, ice sheet, or ice field. Such glaciers usually originate in a cirque and may flow down into a valley (Section 6.2).

7.3. Late Noachian/early Hesperian glacial landscape versus Amazonian VFFs

An important point to discuss is the difference between late Noachian/early Hesperian glacial landscape versus Amazonian VFFs. Even if they are both form by glacial processes, their distribution and their formation conditions are different. These differences are mainly controled by the orbital parameters and atmospheric conditions that are completely different between the late Amazonian and the late Noachain/early Hesperian. Several studies indicate that the formation of VFF seems to be linked with an orbital obliquity increase (Madeleine et al., 2009; Hubbard et al., 2011; Souness and Hubbard, 2012). In fact, Amazonian climatic models suggested that an atmospheric pressure of 0.007 bar and high (45°) to medium obliquity (30°) are favourable conditions to form VFFs (Montmessin, 2004; Forget, 2006). Moreover, the geomorphologic mapping of these features, show that they are only locally found between 30° to 50° in latitudes, on crater slopes $>$ 20° (Milliken, 2003; Hubbard et al., 2011; Souness and Hubbard, 2012; Hubbard et al., 2014). So the VFFs have a latitudinal and slope dependence and are formed under particular conditions. The late Noachain/early Hesperian glacial landscape we found in the three sites are at elevations $>$ 1000 m (Fig. 14). Climatic models suggested that, with an obliquity of 45° and under a 1 bar CO_2 atmosphere with cloud, radiative effects and active water cycle, water ice could deposit in area $>$ 1000 m in elevation without latitudinal dependence (Forget et al., 2013; Wordsworth et al., 2013). At this high obliquity, the exchange in water ice and CO_2 become more intense, and surface ice are predicted to become stable even at equatorial latitudes (Conway et al., 2018). Moreover, even if we analyzed only three sites on Terra Sabaea, a preliminary mapping of the whole area seems to indicate that more structures seems to have glacial landscape. A futur detailed study of these features will be done in order to characterize the regional distribution of these landscapes. However, our observations linked with the climatic models suggested that the late Noachian/early Hesperian glacial landscape have an altitudinal dependence and are formed under less particular conditions and on larger scale than VFFs.

7.4. Paleoclimatic implications

Almost all the valleys identified in this study as being glacial in origin are located at elevations between 1000 m and 3000 m (Fig. 14). The glacial valley elevations we found are consistent with the previous modeling studies which predicted the deposition of water ice at elevations $>$ 1000 m during the late Noachian (Wordsworth et al., 2013; Bouley. et al., 2016). Nevertheless, on Earth, the equilibrium line altitude (ELA)

for a glacier, which separates area where the ice is stable (upper accumulation zone) from the area where the ice is not stable (lower ablation zone), is approximated as the elevation which corresponds to the 1/3 of the length of the valley (Anderson et al., 2006). If we apply this rule to Terra Sabaea, we find that the elevation of the ELA is at about 1800 m for Dawes crater and 2000 m for Crater 1. These paleo-ELA are higher than the predicted 1000 m elevation stability of ice in the climatic models (Wordsworth et al., 2013; Bouley. et al., 2016).

Ramirez and Craddock (2018) reviewed the debate between the wet and warm early martian climate versus the icy highlands scenario. They suggested that the icy highlands scenario is not possible because of the complete absence of glacial features in Noachian terrains. However, our study demonstrates, for the first time the presence of a glacial landscape composed of glacial valleys associated with glacial cirques in Noachian terrains in the south of Terra Sabaea (Fig. 18). The observed sequence of Al-bearing clays being deposited over Mg-Fe-bearing clays in ancient terrains has also been interpreted to be consistent with a frozen early martian surface (Ehlmann et al., 2011).

Independently of the debate, we suggest that these two climates could have coexisted. On the Earth, it is common to find places where the ice is stable at high elevation and not stable at lower elevation. The southern highlands have evidence of glacial landscape at elevations $>$ 1000 m, but also some nearby fluvial valley networks at elevations $<$ 1000 m, these two kinds of landscapes seem to be linked together by their ages and their distribution. The catchment of Naktong Vallis, one of the biggest valley networks on Mars (located at 850 km at the north of Dawes crater at an elevation of 1200 m), extends up to a large plateau located at more than 2000 m elevation near Dawes crater (Bouley et al., 2009) and is dated at 3.6 Ga (Fassett and Head, 2008a; Bouley et al., 2009; Bouley. and Craddock, 2014). This age is consistent with the age found for the glacial landscape in Dawes crater and show that the liquid and water ice could have coexisted. Moreover, the glacial landscapes are located at altitudes where the valley network density is known to be low (elevations $>$ 1500 m; Table 10 and Fig. 2a). For elevations $<$ 1500 m the valley network density is known to be higher (Fig. 2a; Bouley et al. 2009). In order to explain this altitudinal relationship between the glacial landscape and the valley networks we propose two hypotheses:

(1) These two climates scenarios are complementary, indeed to form these two types of valley morphologies, a high atmospheric humidity is necessary. Several studies have proposed snowfall and melting snow as the source of water for the valley networks (Head et al., 2005; Bouley et al., 2009; Fastook et al., 2012). Moreover, at the lowest elevations ($<$1500 m), the high density of V-shaped valleys, suggests that precipitation played

a role in their formation (Carr, 1995; Baker, 2001; Bibring et al., 2006; Ramirez and Craddock, 2018). Thus, at higher elevations ($>$ 1500 m), snow could have accumulated to form glaciers. We propose that the martian climate during the late Noachian/early Hesperian was characterized by glaciated highlands at $>$ 1500 m according to the glacial landscape we highlighted and temperate lowlands at $<$ 1500 m where liquid water was stable. Thus, a water cycle similar to the Earth could have existed allowing the deposition of snow and glacier formation in the highlands and the precipitation of liquid water for an elevation $<$ 1500 m.

(2) The variations in Mars' orbital obliquity could have changed the global climate and created glacial-interglacial cycles (Laskar et al., 2004). During cold climate periods accumulation and preservation of large amount of water ice could have occured thus forming glacial landscape at elevations $>$ 1500 m. Then during interglacial periods this ice could have melted and liquid water flowed down shaping the valley networks at an elevations $<$ 1500 m.

In any case, we suggest that the melting of ice could be an important factor to consider for valley network formation. The glaciated highlands could allow the formation of local ice sheet around craters where we found glacial landsapes. We suggest that, the ice flowed down on the inner crater slopes to form alpine glacier and shaped the glacial valleys. But outside the crater, where the slope is gentle and where we did not observe alpine glacier morphologies, these supposed local ice sheet could have melted (Fastook and Head, 2015). This melting water could be a source and/or a reservoir of lowest elevations valley networks and feed the open-bassin lake observed in this area by Fassett and Head (2008b). These scenarios would be sufficient to explain most of the valley networks, glacial landscape, and geology in Terra Sabaea. The water liberated could have contributed to the formation of valley networks and the hydration of the soil. Our geomorphological observations provide evidence for a glaciated highlands $>$ 1500 m and temperate lowlands $<$ 1500 m during the late Noachian/ early Hesperian in Terra Sabaea. These results and interpretations are verified in our study area, and bring new elements to the debate about the early Mars climate, but we did not apllied our method to the entire highlands in Terra Sabaea. However, a preliminary mapping have been done and it seems like other impact crater presents morphologies similar to those described in this study. A future study in the whole highlands $>$ 1500 m, applying this method, will be done to better constrain the distribution of this supposed glacial landscape and the link they could have with the martian paleo-climate.

8. Conclusion

Our morphometrical analyses allowed us to identify glacial valleys and glacial cirques distributed across three sites in Terra Sabaea. These glacial landforms have similar characteristics to glacial landforms on Earth. The altitude of this glacial landscape is > 1000 m in agreement with numerical climate simulations that have predicted deposition of ice in the southern hemisphere during the late Noachian. We constrain the timing of the formation of these glacial landscapes to about 3.6 Ga, which corresponds to the late Noachian/early Hesperian. This study supports a glacial erosive agent for the origin of these valleys and brings the first morphometric evidence of an ancient glacial landscape composed of glacial valleys associated with glacial cirques in the southern highlands. Finding similar glacial landscapes in other impact craters or in the inter-crater plains in the southern highlands would allow better constraint on the distribution of the ice for early Mars.

Acknowledgments

The authors acknowledge the CTX Team for the availability of the data on the web site `http://ode.rsl.wustl.edu/mars/` and the HRSC Team of the German Aerospace Center (DLR) Berlin, who provided map projected HRSC DEM data. We acknowledge the Orsay Planetary Picture Library for the data provided and images processing (`http://fototek.geol.u-psud.fr`). Authors are funded by the Programme National de Planétologie (PNP) of Centre National de la Recherche Scientifique/Institut National des Sciences de l'Univers, and the Centre National d'Etudes Spatiales (CNES). The authors also acknowledge Pierre Lahitte for the terrestrial DEM of Chamonix valley. The authors are very grateful to the two reviewers, Susan Conway and Ian S. Evans, for their very constructive comments and suggestions that have improved the work presented here.

References

Amerson, B. E., Montgomery, D. R., Meyer, G., 2008. Relative size of fluvial and glaciated valleys in central idaho. Geomorphology 93 (3-4), 537–547, doi: 10.1016/j.geomorph.2007.04.001.

Anderson, R. S., Molnar, P., Kessler, M. A., 2006. Features of glacial valley profiles simply explained. Journal of Geophysical Research 111 (F1), doi: 10.1029/2005jf000344.

Andersson, G., 1998. Genesis of hummocky moraine in the bolmen area, southwestern sweden. Boreas 27 (1), 55–67, doi: 10.1111/j.1502-3885.1998.tb00867.x.

Arfstrom, J., Hartmann, W. K., 2005. Martian flow features, moraine-like ridges, and gullies: Terrestrial analogs and interrelationships. Icarus 174 (2), 321–335, doi: 10.1016/j.icarus.2004.05.026.

Augustinus, P. C., 1992. Outlet glacier trough size-drainage area relationships, fiordland, new zealand. Geomorphology 4 (5), 347–361, doi: 10.1016/0169-555x(92)90028-m.

Baker, V. R., 2001. Water and the martian landscape. Nature 412 (6843), 228–236, doi: 10.1038/35084172.

Barr, I. D., Spagnolo, M., 2015. Glacial cirques as palaeoenvironmental indicators: Their potential and limitations. Earth-Science Reviews 151, 48–78, doi: 10.1016/j.earscirev.2015.10.004.

Bennett, M., Glasser, N., 2009. Glacial Geology. John Wiley and Sons Ltd,

Bennett, M., Glasser, N., 2011. Glacial Geology: Ice Sheets and Landforms. Wiley.
URL https://books.google.fr/books?id=p6X0M5hAQj8C

Bibring, J.-P., Langevin, Y., Mustard, J. F., Poulet, F., Arvidson, R., Gendrin, A., Gondet, B., Mangold, N., Pinet, P., Forget, F., Berthe, M., Bibring, J.-P., Gendrin, A., Gomez, C., Gondet, B., Jouglet, D., Poulet, F., Soufflot, A., Vincendon, M., Combes, M., Drossart, P., Encrenaz, T., Fouchet, T., Merchiorri, R., Belluci, G., Altieri, F., Formisano, V., Capaccioni, F., Cerroni, P., Coradini, A., Fonti, S., Korablev, O., Kottsov, V., Ignatiev, N., Moroz, V., Titov, D., Zasova, L., Loiseau, D., Mangold, N., Pinet, P., Doute, S., Schmitt, B., Sotin, C., Hauber, E., Hoffmann, H., Jaumann, R., Keller, U., Arvidson, R., Mustard, J. F., Duxbury, T., Forget, F., and, G. N., 2006. Global mineralogical and aqueous mars history derived from OMEGA/mars express data. Science 312 (5772), 400–404, doi: 10.1126/science.1122659.

Bouley., Craddock, R. A., 2014. Age dates of valley network drainage basins and subbasins within sabae and arabia terrae, mars. Journal of Geophysical Research: Planets 119 (6), 1302–1310, doi: 10.1002/2013JE004571.

Bouley, S., Ansan, V., Mangold, N., Masson, P., Neukum, G., 2009. Fluvial morphology of naktong vallis, mars: A late activity with multiple processes. Planetary and Space Science 57 (8-9), 982–999, doi: 10.1016/j.pss.2009.01.015.

Bouley., S., Baratoux, D., Matsuyama, I., Forget, F., Séjourné, A., Turbet, M., Costard, F., 2016. Late tharsis formation and implications for early mars. Nature 531 (7594), 344–347, doi: 10.1038/nature17171.

Brennand, T. A., 2000. Deglacial meltwater drainage and glaciodynamics: inferences from laurentide eskers, canada. Geomorphology 32 (3-4), 263–293, doi: 10.1016/s0169-555x(99)00100-2.

Butcher, F. E., Conway, S. J., Arnold, N. S., 2016. Are the dorsa argentea on mars eskers? Icarus 275, 65–84, doi:10.1016/j.icarus.2016.03.028.

Carr, M., 1995. The martian drainage system and the origin of valley networks and fretted channels. Journal of Geophysical Research 100 (E4), 7479, doi: 10.1029/95je00260.

Carr, M., Malin, M. C., 2000. Meter-scale characteristics of martian channels and valleys. Icarus 146 (2), 366–386, doi: 10.1006/icar.2000.6428.

Carr, M. H., Head, J. W., 2010. Geologic history of mars. Earth and Planetary Science Letters 294 (3-4), 185–203, doi: 10.1016/j.epsl.2009.06.042.

Cogley, J., Arendt, A., Bauder, A., Braithwaite, R., Hock, R., Jansson, P., Kaser, G., Moller, M., Nicholson, L., Rasmussen, L., Zemp, M., 2010. Glossary of glacier mass balance and related terms. Vol. 86 of IHP-VII Technical Documents in Hydrology. UNESCO (IHP Secretariat, Division of Water Sciences.

Conway, S. J., Butcher, F. E., de Haas, T., Deijns, A. A., Grindrod, P. M., Davis, J. M., 2018. Glacial and gully erosion on mars: A terrestrial perspective. Geomorphology 318, 26–57, doi:10.1016/j.geomorph.2018.05.019.

Corti, G., Cocco, S., Basili, M., Cioci, C., Warburton, J., Agnelli, A., 2012. Soil formation in kettle holes from high altitudes in central apennines, italy. Geoderma 170, 280–294, doi:10.1016/j.geoderma.2011.10.016.

Craddock, R. A., Howard, A. D., 2002. The case for rainfall on a warm, wet early mars. Journal of Geophysical Research: Planets 107 (E11), 21–1–21–36, doi: 10.1029/2001je001505.

de Martonne, E., 1910. L'érosion glaciaire et la formation des vallées alpines. Annales de Géographie 19 (106), 289–317.

de Martonne, E., 1911. Fjords, cirques, vallées alpines et lacs subalpins. Annales de Géographie 10 (52), 289–294.

Delmas, M., Gunnell, Y., Calvet, M., 2015. A critical appraisal of allometric growth among alpine cirques based on multivariate statistics and spatial analysis. Geomorphology 228, 637–652, doi: 10.1016/j.geomorph.2014.10.021.

Ehlmann, B. L., Mustard, J. F., Murchie, S. L., Bibring, J.-P., Meunier, A., Fraeman, A. A., Langevin, Y., 2011. Subsurface water and clay mineral formation during the early history of mars. Nature 479 (7371), 53–60, doi: 10.1038/nature10582.

Evans, I. S., 2010. Allometry, scaling and scale-specificity of cirques, landslides and other landforms. Transactions,Japanese Geomorphological Union 31 (2), 133–153.
URL https://ci.nii.ac.jp/naid/110007621737/en/

Evans, I. S., Cox, N. J., 2017. Comparability of cirque size and shape measures between regions and between researchers. Zeitschrift fÃŒr Geomorphologie, Supplementary Issues 61 (2), 81–103.

Ewertowski, M. W., Tomczyk, A. M., 2015. Quantification of the ice-cored moraines' short-term dynamics in the high-arctic glaciers ebbabreen and ragnarbreen, petuniabukta, svalbard. Geomorphology 234, 211–227, doi: 10.1016/j.geomorph.2015.01.023.

Fassett, C. I., Head, J. W., 2008a. The timing of martian valley network activity: Constraints from buffered crater counting. Icarus 195 (1), 61–89, doi: 10.1016/j.icarus.2007.12.009.

Fassett, C. I., Head, J. W., 2008b. Valley network-fed, open-basin lakes on mars: Distribution and implications for noachian surface and subsurface hydrology. Icarus 198 (1), 37–56, doi: 10.1016/j.icarus.2008.06.016.

Fastook, J. L., Head, J. W., 2015. Glaciation in the late noachian icy highlands: Ice accumulation, distribution, flow rates, basal melting, and top-down melting rates and patterns. Planetary and Space Science 106, 82–98, https://doi.org/10.1016/j.pss.2014.11.028.

Fastook, J. L., Head, J. W., Marchant, D. R., Forget, F., Madeleine, J.-B., 2012. Early mars climate near the noachian–hesperian boundary: Independent evidence for cold conditions from basal melting of the south polar ice sheet (dorsa argentea formation) and implications for valley network formation. Icarus 219 (1), 25–40, doi: 10.1016/j.icarus.2012.02.013.

Fitzsimons, S. J., 1991. Supraglacial eskers in antarctica. Geomorphology 4 (3-4), 293–299, doi: 10.1016/0169-555x(91)90011-x.

Forget, F., 2006. Formation of glaciers on mars by atmospheric precipitation at high obliquity. Science 311 (5759), 368–371, doi: 10.1126/science.1120335.

Forget, F., Wordsworth, R., Millour, E., Madeleine, J.-B., Kerber, L., Leconte, J., Marcq, E., Haberle, R., 2013. 3d modelling of the early martian climate under a denser co2 atmosphere: Temperatures and co2 ice clouds. Icarus.

Frezzotti, M., Orombelli, G., 2013. Glaciers and ice sheets: current status and trends. Rendiconti Lincei 25 (1), 59–70, doi: 10.1007/s12210-013-0255-z.

Gallagher, C., Balme, M., 2015. Eskers in a complete, wet-based glacial system in the phlegra montes region, mars. Earth and Planetary Science Letters 431, 96–109, doi:10.1016/j.epsl.2015.09.023.

Gourronc, M., Bourgeois, O., Mège, D., Pochat, S., Bultel, B., Massé, M., Deit, L. L., Mouélic, S. L., Mercier, D., 2014. One million cubic kilometers of fossil ice in valles marineris: Relicts of a 3.5gy old glacial landsystem along the martian equator. Geomorphology 204, 235–255, doi: 10.1016/j.geomorph.2013.08.009.

Graf, W. L., 1970. The geomorphology of the glacial valley cross section. Arctic and Alpine Research 2 (4), 303, doi: 10.2307/1550243.

Graf, W. L., 1976. Cirques as glacier locations. Arctic and Alpine Research 8 (1), 79, doi: 10.2307/1550611.

Gulick, V. C., 2001. Origin of the valley networks on mars: a hydrological perspective. Geomorphology 37 (3-4), 241–268, doi: 10.1016/s0169-555x(00)00086-6.

Gwinner, K., Jaumann, R., Hauber, E., Hoffmann, H., Heipke, C., Oberst, J., Neukum, G., Ansan, V., Bostelmann, J., Dumke, A., Elgner, S., Erkeling, G., Fueten, F., Hiesinger, H., Hoekzema, N., Kersten, E., Loizeau, D., Matz, K.-D., McGuire, P., Mertens, V., Michael, G., Pasewaldt, A., Pinet, P., Preusker,

F., Reiss, D., Roatsch, T., Schmidt, R., Scholten, F., Spiegel, M., Stesky, R., Tirsch, D., van Gasselt, S., Walter, S., WÃ€hlisch, M., Willner, K., 2016. The high resolution stereo camera (HRSC) of mars express and its approach to science analysis and mapping for mars and its satellites. Planetary and Space Science 126, 93–138, doi: 10.1016/j.pss.2016.02.014.

Hargitai, H., Kereszturi, Á. (Eds.), 2015. Encyclopedia of Planetary Landforms. Springer New York.

Hartmann, W. K., 2005. Martian cratering 8: Isochron refinement and the chronology of mars. Icarus 174 (2), 294–320, doi: 10.1016/j.icarus.2004.11.023.

Hartmann, W. K., Neukum, G., 2001. Cratering chronology and the evolution of mars. Space Science Reviews 96 (1/4), 165–194, doi: 10.1023/a:1011945222010.

Head, J. W., Marchant, D. R., 2014. The climate history of early mars: insights from the antarctic McMurdo dry valleys hydrologic system. Antarctic Science 26 (06), 774–800, doi: 10.1017/s0954102014000686.

Head, J. W., Neukum, G., Jaumann, R., Hiesinger, H., Hauber, E., Carr, M., Masson, P., Foing, B., Hoffmann, H., Kreslavsky, M., Werner, S., Milkovich, S., van Gasselt, S., 2005. Tropical to mid-latitude snow and ice accumulation, flow and glaciation on mars. Nature 434 (7031), 346–351, doi: 10.1038/nature03359.

Hobbs, S., Clarke, J., Paull, D., 2016. Analysis of crater valleys, noachis terra, mars: Evidence of fluvial and glacial processes. Geomorphology 261, 244–272, doi: 10.1016/j.geomorph.2016.02.027.

Holt, J. W., Safaeinili, A., Plaut, J. J., Head, J. W., Phillips, R. J., Seu, R., Kempf, S. D., Choudhary, P., Young, D. A., Putzig, N. E., Biccari, D., Gim, Y., 2008. Radar sounding evidence for buried glaciers in the southern mid-latitudes of mars. Science 322 (5905), 1235–1238, doi: 10.1126/science.1164246.

Hubbard, B., Milliken, R. E., Kargel, J. S., Limaye, A., Souness, C., 2011. Geomorphological characterisation and interpretation of a mid-latitude glacier-like form: Hellas planitia, mars. Icarus 211 (1), 330–346, doi: 10.1016/j.icarus.2010.10.021.

Hubbard, B., Souness, C., Brough, S., 2014. Glacier-like forms on mars. The Cryosphere 8 (6), 2047–2061, doi: 10.5194/tc-8-2047-2014.

Hynek, B. M., Beach, M., Hoke, M. R. T., 2010. Updated global map of martian valley networks and implications for climate and hydrologic processes. Journal of Geophysical Research 115 (E9), doi: 10.1029/2009je003548.

Ivanov, B. A., 2001. Mars/moon cratering rate ratio estimates. In: Space Sciences Series of ISSI. Springer Netherlands, pp. 87–104, doi: 10.1007/978-94-017-1035-0.

Jackson, Julia A., ., Mehl, J. P., Neuendorf, K. K. E., Institute, A. G., 2005. Glossary of geology, 5th Edition. Alexandria, Va. : American Geological Institute.
URL http://deposit.ddb.de/cgi-bin/dokserv?id=2669188&prov=M&dok_var=1&dok_ext=htm

Johnson, W. D., 1904. The profile of maturity in alpine glacial erosion. The Journal of Geology 12 (7), 569–578, doi: 10.1086/621181.

Kargel, J. S., Strom, R. G., 1992. Ancient glaciation on mars. Geology 20 (1), 3, doi: http://dx.doi.org/10.1130/0091-7613(1992)020<0003:AGOM>2.3.CO;2.
URL +http://dx.doi.org/10.1130/0091-7613(1992)020<0003:AGOM>2.3.CO;2

Kneissl, T., van Gasselt, S., Neukum, G., 2011. Map-projection-independent crater size-frequency determination in GIS environments—new software tool for ArcGIS. Planetary and Space Science 59 (11-12), 1243–1254, doi: 10.1016/j.pss.2010.03.015.

Laskar, J., Correia, A., Gastineau, M., Joutel, F., Levrard, B., Robutel, P., aug 2004. Long term evolution and chaotic diffusion of the insolation quantities of mars. Icarus 170 (2), 343–364.

Léonard, J., Richard, G., 2004. Estimation of runoff critical shear stress for soil erosion from soil shear strength. CATENA 57 (3), 233–249, doi: 10.1016/j.catena.2003.11.007.

Livers, B., Wohl, E., 2015. An evaluation of stream characteristics in glacial versus fluvial process domains in the colorado front range. Geomorphology 231, 72–82, doi: 10.1016/j.geomorph.2014.12.003.

Madeleine, J.-B., Forget, F., Head, J. W., Levrard, B., Montmessin, F., Millour, E., oct 2009. Amazonian northern mid-latitude glaciation on mars: A proposed climate scenario. Icarus 203 (2), 390–405.

Malin, M. C., Edgett, K. S., 2001. Mars global surveyor mars orbiter camera: Interplanetary cruise through primary mission. Journal of Geophysical Research: Planets 106 (E10), 23429–23570, doi: 10.1029/2000je001455.

Mège, D., Bourgeois, O., 2011. Equatorial glaciations on mars revealed by gravitational collapse of valles marineris wallslopes. Earth and Planetary Science Letters 310 (3-4), 182–191, doi: 10.1016/j.epsl.2011.08.030.

Milliken, R. E., 2003. Viscous flow features on the surface of mars: Observations from high-resolution mars orbiter camera (MOC) images. Journal of Geophysical Research 108 (E6), doi: 10.1029/2002je002005.

Montgomery, D. R., 2002. Valley formation by fluvial and glacial erosion. Geology 30 (11), 1047, doi: 10.1130/0091-7613(2002)030<1047:vfbfag>2.0.co;2.

Montmessin, F., 2004. Origin and role of water ice clouds in the martian water cycle as inferred from a general circulation model. Journal of Geophysical Research 109 (E10), doi: 10.1029/2004JE002284.

Moore, J. M., 2005. Large alluvial fans on mars. Journal of Geophysical Research 110 (E4), doi: 10.1029/2004je002352.

Nagle, G., Witherick, M., 2002. Cold Environments: Processes and Outcomes (Epics). Nelson Thornes.
URL https://www.amazon.com/Cold-Environments-Processes-Outcomes-Epics/dp/0748758216?SubscriptionId=AKIAIOBINVZYXZQZ2U3A&tag=chimbori05-20&linkCode=xm2&camp=2025&creative=165953&creativeASIN=0748758216

Olyphant, G. A., 1981. Allometry and cirque evolution. Geological Society of America Bulletin 92 (9), 679.

Penck, A., 1905. Glacial features in the surface of the alps. The Journal of Geology 13 (1), 1–19, doi: http://www.jstor.org/stable/30066319.
URL http://www.jstor.org/stable/30066319

Phillips, R. J., 2001. Ancient geodynamics and global-scale hydrology on mars. Science 291 (5513), 2587–2591, doi: 10.1126/science.1058701.

Plaut, J. J., Safaeinili, A., Holt, J. W., Phillips, R. J., Head, J. W., Seu, R., Putzig, N. E., Frigeri, A., 2009. Radar evidence for ice in lobate debris aprons in the mid-northern latitudes of mars. Geophysical Research Letters 36 (2), n/a–n/a, doi:10.1029/2008GL036379.

Ramirez, R. M., Craddock, R. A., 2018. The geological and climatological case for a warmer and wetter early mars. Nature Geoscience 11 (4), 230–237, doi: 10.1038/s41561-018-0093-9.

Roberts, M. C., Rood, K. M., 1984. The role of the ice contributing area in the morphology of transverse fjords, british columbia. Geografiska Annaler. Series A, Physical Geography 66 (4), 381–393, doi: http://www.jstor.org/stable/520858.
URL http://www.jstor.org/stable/520858

Segura, T. L., 2002. Environmental effects of large impacts on mars. Science 298 (5600), 1977–1980, doi: 10.1126/science.1073586.

Smith, D. E., Zuber, M. T., Frey, H. V., Garvin, J. B., Head, J. W., Muhleman, D. O., Pettengill, G. H., Phillips, R. J., Solomon, S. C., Zwally, H. J., Banerdt, W. B., Duxbury, T. C., Golombek, M. P., Lemoine, F. G., Neumann, G. A., Rowlands, D. D., Aharonson, O., Ford, P. G., Ivanov, A. B., Johnson, C. L., McGovern, P. J., Abshire, J. B., Afzal, R. S., Sun, X., 2001. Mars orbiter laser altimeter: Experiment summary after the first year of global mapping of mars. Journal of Geophysical Research: Planets 106 (E10), 23689–23722, doi: 10.1029/2000je001364.

Souness, C., Hubbard, B., 2012. Mid-latitude glaciation on mars. Progress in Physical Geography 36 (2), 238–261, doi: 10.1177/0309133312436570.

Squyres, S. W., 1979. The distribution of lobate debris aprons and similar flows on mars. Journal of Geophysical Research 84 (B14), 8087, doi: 10.1029/jb084ib14p08087.

Tanaka, K. L., 1986. The stratigraphy of mars. Journal of Geophysical Research 91 (B13), E139, doi: 10.1029/jb091ib13p0e139.

Tanaka, K. L., 2014. Geological map of marsHttp://dx.doi.org/10.3133/sim3292.
URL http://dx.doi.org/10.3133/sim3292.

Wordsworth, R., Forget, F., Millour, E., Head, J., Madeleine, J.-B., Charnay, B., 2013. Global modelling of the early martian climate under a denser CO2 atmosphere: Water cycle and ice evolution. Icarus 222 (1), 1–19, doi: 10.1016/j.icarus.2012.09.036.

Zemp, M., Haeberli, W., Paul, F., 2011. Vanishing glaciers in the european alps. Doi: 10.5167/uzh-83973.

Zimmer, P. D., Gabet, E. J., 2018. Assessing glacial modification of bedrock valleys using a novel approach. Geomorphology 318, 336–347, https://doi.org/10.1016/j.geomorph.2018.06.021.

Supplementary material

CTX/ HRSC

Studied Structures	CTX	HRSC
Dawes crater	B21_017816_1708_XN_09S322W B20_017394_1735_XN_06S321W B19_017104_1709_XN_09S323W P17_007742_1708_XN_09S323W P14_006529_1708_XN_09S321W P13_006239_1706_XN_09S323W P11_005461_1706_XI_09S323W P11_005395_1717_XI_08S320W P11_005250_1714_XI_08S322W G23_027376_1684_XN_11S320W B18_016827_1684_XN_11S319W G22_026743_1724_XN_07S321W D15_033257_1689_XN_11S319W D10_031055_1703_XN_09S320W P21_009179_1697_XN_10S322W G01_018739_1714_XN_08S322W B01_010102_1699_XN_10S321W D07_030132_1718_XN_08S320W	h1961_0000_bl3 h1950_0000_bl3 h1928_0000_re3 h1928_0000_nd3
Crater 1	J01_044980_1713_XN_08S316W B08_012594_1713_XN_08S316W F02_036448_1716_XN_08S317W D01_027455_1729_XN_07S318W B19_016906_1705_XN_09S317W B16_015917_1710_XN_09S317W P15_006753_1707_XN_09S317W F03_037015_1729_XN_07S318W G02_019174_1705_XN_09S318W	h5184_0000_da4 h5202_0000_da4
GLF-crater	P07_003589_1466_XN_33S331W B11_013966_1476_XN_32S331W B09_013254_1466_XI_33S331W B06_011909_1480_XN_32S332W	h2540_0000_nd3 h2540_0000_da4 h2540_0000_nd3 h2540_0000_bl3 h2540_0000_gr3
Positive relief	P12_005619_1752_XI_04S317W D22_035815_1762_XN_03S318W G19_025833_1759_XN_04S317W F05_037582_1752_XN_04S316W F05_037793_1760_XN_04S318W F04_037516_1812_XN_01N317W D15_033191_1757_XN_04S318W	h5184_0000_gr3 h8412_0000_ir3
Bakhuysen crater	G05_020309_1568_XN_23S343W G12_022933_1578_XI_22S344W B18_016551_1566_XN_23S344W B20_017263_1573_XI_22S343W B18_016617_1562_XI_23S345W B17_016195_1563_XN_23S345W P11_005475_1569_XN_23S343W	h6445_0000_da4 h6445_0000_gr3 h6488_0000_dt4 h6488_0000_da4

Table 3. CTX images and HRSC elevation data used for this study

Bakhuysen valleys

Length 0% [m	Length 25%	Length 50%	Length 75%	Length 100%	Width 0% [m]	Width 25%	Width 50%	Width 75%	Width 100%	Average Width	Surface [m²]	Slope [°]	Depth [m]	Elevation [m]	Cumulative volume [m^3]	Cross-section 0 %[m²]	Cross-section 25%	Cross-section50%	Cross-section 75%	Cross-section 100%	Average cross-section
0.00	4767.50	9535.00	14302.50	19070.00	146.00	679.00	1854.00	704.00	898.00	856.20	20574190.00	4.13	11.67	194.96	99073075.16		1431.51	9085.14	5069.05		5195.23
0.00	2966.50	5933.00	8899.50	11866.00	799.00	1019.00	941.00	1669.00	305.00	946.60	13422022.00	5.38	37.00	186.68	2230588915.27	13697.70	14190.05	32316.76	18610.12	15176.14	18798.16
0.00	2340.75	4681.50	7022.25	9363.00	169.00	775.00	537.00	777.00	216.00	494.80	5571520.00	3.12	19.33	190.73	90406668.93		2452.35	6810.03	19704.83		9655.74
0.00	3204.50	6409.00	9613.50	12818.00	708.00	1036.00	775.00	1692.00	470.00	936.20	14495773.00	2.59	12.80	178.99	673422271.27	4809.40	17058.80	962.23	1833.96	1604.25	5253.73
0.00	1711.00	3422.00	5133.00	6844.00	0.00	280.00	215.00	531.00	328.00	270.80	2285268.00	3.61	18.75	155.88	67814193.98	2414.44	1081.31		29087.12	7051.38	9908.56
0.00	1610.75	3221.50	4832.25	6443.00	35.00	216.00	340.00	419.00	409.00	283.80	2430728.00	2.73	7.50	135.29	26066572.69		1470.44	3997.20	3382.97	7332.27	4045.72
0.00	1966.75	3933.50	5900.25	7867.00	217.00	138.00	413.00	255.00	40.00	212.60	1885311.00	1.12	3.00	121.40	7224885.30	1168.92		1457.11	129.11		918.38
0.00	2419.00	4838.00	7257.00	9676.00	382.00	488.00	562.00	699.00	464.00	521.00	5747098.00	5.33	16.75	151.58	98382790.13	768.29	31506.20	2814.58	4584.91		10168.75
0.00	5231.50	10463.00	15694.50	20926.00	424.00	488.00	1423.00	728.00	318.00	676.20	14851986.00	6.81	32.40	146.63	314052422.27	8787.63	14710.17	20919.14	17115.41	13508.46	15007.76
0.00	4589.25	9178.50	13767.75	18357.00	578.00	409.00	623.00	779.00	0.00	477.80	11375554.00	4.99	24.60	140.18	270262925.04	3742.36	4921.90	11278.77	46964.21	6705.80	14722.61
0.00	2520.50	5041.00	7561.50	10082.00	285.00	619.00	354.00	579.00	0.00	367.40	5191379.00	4.30	12.25	168.00	38471751.10	368.30	5175.05		3180.16	6550.03	3815.88
0.00	3343.25	6686.50	10029.75	13373.00	487.00	489.00	590.00	888.00	214.00	533.60	7831643.00	3.96	14.20	170.96	53740022.58	1139.24	3410.47	2857.75	11938.74	746.53	4018.55
0.00	2488.00	4976.00	7464.00	9952.00	523.00	818.00	302.00	536.00	219.00	479.60	5467494.00	4.38	16.67	166.20	75997687.11	9092.26	6838.39		6978.62		7636.42
0.00	3194.00	6388.00	9582.00	12776.00	168.00	753.00	979.00	1870.00	858.00	925.60	15555448.00	3.70	10.00	121.34	306722288.87	2793.59	1623.92	2784.81			2400.77
0.00	1459.75	2919.50	4379.25	5839.00	0.00	500.00	777.00	1094.00	628.00	599.80	4405470.00	4.55	30.00	180.92	633611136.29		7263.70	14439.04			10851.37
0.00	2674.75	5349.50	8024.25	10699.00	0.00	549.00	292.00	518.00	368.00	345.40	5401413.00	4.19	9.00	171.62	26150891.07		3005.97	1882.51			2444.24
0.00	4059.00	4118.00	6177.00	8236.00	370.00	475.00	304.00	394.00	161.00	340.80	3308866.00	3.21	10.00	164.56	21346406.27	2037.24	6705.92		387.35	1236.85	2591.84
0.00	1824.75	1849.50	2774.25	3699.00	144.00	574.00	848.00	1747.00	343.00	731.20	3926979.00	4.25	36.50	156.36	50373799.97		3910.04	23326.40			13618.22
0.00	2417.25	4834.50	7251.75	9669.00	601.00	588.00	819.00	801.00	393.00	640.40	6778504.00	2.92	9.80	168.26	238257133.69	249.16	538.09	1041.08	6584.76	3907.58	2464.14
0.00	857.25	1714.50	2571.75	3429.00	302.00	447.00	345.00	314.00	318.00	345.20	1292484.00	2.04	4.25	169.95	26671611.99	744.59	107.13	1682.81	577.29		777.96
0.00	1415.50	2831.00	4246.50	5662.00	0.00	282.00	430.00	434.00	605.00	350.20	2013353.00	2.18	5.35	171.76	97144408.04	2737.56	2329.28		328.83	1467.21	1715.72
0.00	1797.00	3594.00	5391.00	7188.00	125.00	705.00	627.00	730.00	196.00	476.60	4139483.00	2.24	3.67	172.98	87141613.67		1466.85		1829.90	351.68	1116.14
0.00	771.75	1543.50	2315.25	3087.00	316.00	701.00	475.00	431.00	145.00	413.60	1509431.00	2.93	5.00	172.80	55665936.03	3049.37		1554.67		805.03	1803.02
0.00	4759.75	9519.50	14279.25	19039.00	0.00	452.00	708.00	908.00	1392.00	692.00	12906052.00	3.43	17.50	177.26	151898372.63		13419.49	2018.74	6277.25	10197.62	7978.27
0.00	1607.25	3214.50	4821.75	6429.00	429.00	422.00	451.00	768.00	159.00	445.80	3670874.00	2.85	10.75	168.90	20938514.11	93.28	1665.73		1548.63	9719.91	3256.89
0.00	4260.25	8520.50	12780.75	17041.00	372.00	496.00	712.00	689.00	286.00	511.00	9315417.00	3.24	17.20	176.74	169070981.26	3930.46		4545.00	26470.04	4740.19	9921.42
0.00	1443.25	2886.50	4329.75	5773.00	224.00	464.00	561.00	838.00	172.00	451.80	3069941.00	3.99	11.50	165.61	12775513.48		2054.64	2148.18	3031.94	1617.14	2212.98
0.00	5204.00	10408.00	15612.00	20816.00	0.00	335.00	533.00	810.00	258.00	387.20	13009437.00	3.94	5.40	165.51	519718O5.86	411.55	5788.24	442.21	5067.92	773.71	2496.72
0.00	1981.50	3963.00	5944.50	7926.00	0.00	364.00	749.00	378.00	221.00	342.40	3570194.00	2.41	11.00	185.33	22076031.48	357.03	1398.45	4768.79	4616.80		2785.27
0.00	1071.25	2142.50	3213.75	4285.00	0.00	273.00	259.00	554.00	201.00	257.40	1435109.00	2.80	8.00	177.96	5809592.36			1355.80			1355.80
0.00	2047.75	4095.50	6143.25	8191.00	316.00	173.00	426.00	550.00	226.00	338.20	3146176.00	2.91	9.50	186.11	20437255.63	323.78	668.84	3144.67	5843.06		2495.09
0.00	3749.25	7498.50	11247.75	14997.00	249.00	574.00	510.00	521.00	305.00	431.80	7436760.00	2.95	17.20	188.46	87715011.15	514.23	8177.87	3475.83	5472.47	11603.78	5848.84
0.00	1667.25	3334.50	5001.75	6669.00	151.00	423.00	396.00	670.00	185.00	365.00	3278810.00	4.67	20.00	177.89	55595597.18		2554.11	12917.56	9539.40		8337.02
0.00	6836.75	13673.50	20510.25	27347.00	261.00	521.00	468.00	701.00	355.00	461.20	16235881.00	3.41	7.25	187.74	834600688.78	1094.20	1792.55	2487.25	6833.57		3051.89
0.00	3314.50	6629.00	9943.50	13258.00	505.00	874.00	680.00	920.00	371.00	670.00	12560229.00	6.18	43.33	161.58	386507991.93		24316.07	37131.26	28726.45		30057.93

Table 4. All measured parameters for Bakhuysen crater valleys

GLF-crater valleys

Length 0% (m)	Length 25%	Length 50%	Length 75%	Length 100%	Width 0% (m)	Width 25%	Width 50 %	Width75%	Width 100%	Average Width	Surface (m²)	Slope (°)	Depth (m)	Elevation (m)	Cumulative volume (m^3)	Cross-section 0 %(m²)	Cross-section 25%	Cross-section50%	Cross-section 75%	Cross-section 100%	Average cross-section
0	1905	3810	5715	7620	1960	2218	2933	3451	823	2277	18847662	9.75	31.5	1223.97	168509799.4	9364.187645		40253.15602	21386.83421	17452.40971	22114.1469
0	321	642	963	1284	1002	922	898	866	187	775	1115347	10.06	17.33333333	919.14	6532732.407	3774.174722	5473.056199	6016.162553			5087.797825
0	417.25	834.5	1251.75	1669	729	817	795	504	158	600.6	1183525	12.58	21.33333333	970.18	18195517.1	4832.653695	16444.49124	11428.99725			10902.04739
0	946.5	1893	2839.5	3786	1394	1743	1727	1033	232	1225.8	5188014	10.2	21.2	1394.92	40468089.14	6988.23667	7825.739966	28128.82881	6121.765095	4379.815541	10688.87722
0	1230	2460	3690	4920	1767	2287	1507	873	560	1398.8	7219922	11.84	17.75	1230.94	39138703.06		13093.4927	6367.15866	3390.931303	8968.501125	7955.020947
0	1158	2316	3474	4632	1278	1657	1318	1162	928	1268.6	6170504	9.79	20.6	962.08	77404024.32	7638.940406	23074.29385	9695.956956	12652.08167	30492.29396	16710.71337
0	1996.75	3993.5	5990.25	7987	484	2073	1679	1367	201	1160.8	11738543	10.75	15	1233.5	42243399.92	3613.855513	3851.95898	3220.406686	12295.91396	3462.963091	5289.019647
0	683.5	1367	2050.5	2734	820	936	1001	909	506	834.4	6880054	16.3	21.33333333	1865.92	29967618.09	4232.985988		12535.3349	16114.94695		10961.08928
0	1762.75	3525.5	5288.25	7051	725	2068	4257	1860	2219	2225.8	3021063	10.1	23.75	1168.23	144455458.1	8388.088974	16136.92809		32886.04865	24537.85392	20487.22991
0	[illegible]	3538.5	5307.75	7077	725	2068	5391	1504	307	1999	3021063	10.1	11.75	1168.23	109241321.5	8388.088974	16136.92809	21499.04704		15720.35951	15436.1059
0	977.5	1955	2932.5	3910	1383	714	1046	675	307	825	3676587	13.05	19.4	1430.93	35555906.22	20062.04219	9428.378441	3786.843451	2600.190391	9590.456299	9093.582154
0	984.5	1969	2953.5	3938	1302	1116	820	1002	629	973.8	10103630	8.04	12.6	1080.21	29153773.81	1204.494125	7373.218483	2575.59583	13330.41705	12532.23923	7403.192943
0	1471	2942	4413	5884	434	1455	1334	3261	1735	1643.8	2955840	10.8	19.4	1412.85	263953549.4	2272.494504	24207.64203	6560.335872	70525.10824	120732.133	44859.54272
0	763	1526	2289	3052	1111	711	836	1091	1040	957.8	7310050	11	14	1315.35	27176550.09	18345.0757	5126.551167	1919.499289	922.2353021	18209.1649	8904.505272
0	1852.75	3705.5	5558.25	7411	459	1205	1085	991	167	781.4	3254711	11	16.5	1664.77	83121906.91	1847.162927	2931.915471		21182.02327	18902.96899	11216.01766
0	1160.5	2321	3481.5	4642	435	991	1056	416	171	613.8	1765629	10.08	19.4	1619.37	45458058.28	9446.425374	10789.3529	9821.577224	7268.129389	11638.38659	9792.774296
0	753.25	1506.5	2259.75	3013	426	601	763	730	159	535.8	897851	10.04	10	1617.64	15741224.4	3354.863344	3787.512801	500.8047323		13254.56144	5224.435579
0	472.5	945	1417.5	1890	382	586	596	347	195	421.2		12.14		1814.67	5589863.556	2881.294784	2541.012748	6030.993361	2461.640381	873.0575502	2957.599765
0	250.75	501.5	752.25	1003	1579	2966	2081	2942	614	2036.4	2216434	10.06	26.25	1353.79	24234788.73	31024.4573	40835.99013	10091.94427		14696.81557	24162.30182
0	693	1386	2079	2772	432	885	833	811	531	698.4	1867649	14.89	12.5	1384.66	19543123.3	5379.230675	5660.515459	5681.6851	11479.32389		7050.188781
0	435.5	871	1306.5	1742	939	983	990	1200	224	867.2	2405623	10.3	24	969.19	16212484.89	2580.485853	5188.514884	12473.44648	25028.14784	1263.517703	9306.822553

Table 5. All measured parameters for GLF-crater valleys

Dawes crater valleys and valley heads

Length 0% (m)	Length 25%	Length 50%	Length 75%	Length 100%	Width 0% (m)	Width 25%	Width 50 %	Width75%	Width 100%	Average Width	Surface (m²)	Slope (°)	Depth (m)	Elevation (m)	Cumulative volume (m^3)	Cross-section 0 %(m²)	Cross-section 25%	Cross-section50%	Cross-section 75%	Cross-section 100%	Average cross-section
0	746.75	1493.5	2240.25	2987		2334	2477	2274		2361.666667	6839779	18.4	55	1909.5	77114176.22	21274.44196	53796.51232	37489.44096	14114.37753	2408.213875	25816.59733
0	1420.25	2840.5	4260.75	5681	183	1707	2477	3636		2000.75	15154448	13.8	47.33333333	1967.42	106551218.7		35319.63822	2613.437005	8913.94801	28175.838	18755.71531
0	1223.5	2447	3670.5	4894	969	1553	801	1249		1143	5784963	9.5	27.4	2529.43	57108013.59	13382.76933	27727.0609	1038.325491	4527.785095		11668.9852
0	483.75	967.5	1451.25	1935	972	850	844	804		867.5	1566515	12.2	35.5	1880.68	19278883.92	6991.274019	5727.553521	9922.386436	17211.77604		9963.247504
0	697.5	1395	2092.5	2790	294	1059	1076	993		855.5	2658901	18.7	28.66666667	1989.7	15637092.65		8946.509827	5971.998047	4565.389951	2934.872997	5604.692706
0	1041.25	2082.5	3123.75	4165	948	1218	1752	1810		1432	6599254	17.3	75.66666667	1973.2	105670459.3	2903.451456	66283.37155	7704.286369	24593.12523		25371.05865
0	1127.25	2254.5	3381.75	4509	1981	1860	578	1043	1080	1308.4	5793246	19.2	37.25	1909.35	88693020.41		45427.14717	6461.261958	23864.70131	2927.768175	19670.21965
0	1671.25	3342.5	5013.75	6685	3459	3787	2773	3190	2097	3061.2	16543137	11.3	77	861.07	740766887.2		71699.3534	97577.29978	163154.261		110810.3047
0	799.5	1599	2398.5	3198	1391	1085	1357	1608		1360.25	4291934	10.8	35.4	1056.06	32680955.95	10365.63566	1873.405551	11706.53087	13333.62002	13816.73652	10219.18572
0	2385.75	4771.5	7157.25	9543		2495	2242	3798		2845	31671560	16.8	56.6	1655.62	268501322.5		58264.77645	21077.79435	21077.79435	12123.41457	28135.94493
0	1580	3160	4740	6320	1386	1160	5504	3057		2776.75	15375475	15.5	70.75	1308.85	223811341.2	4188.741661	23684.91984	43064.61252	70714.47355		35413.18689
0	1161.75	2323.5	3485.25	4647		2651	2250	2544	3082	2631.75	12394570	14.2	83.33333333	1024.82	155537962.6		61747.8743	35823.01332	26463.51098	9848.074035	33470.61816
0	1747.75	3495.5	5243.25	6991	1783	2381	2510	1704	804	1836.4	15081571	14.2	72.33333333	2240.1	279807286.5	22487.30301	80620.63003	16963.85348			40023.92884
0	942.5	1885	2827.5	3770	2340	1789	1635	1983		1936.75	6229162	12.5	52.75	1648.91	76550500.12		27562.45482	20789.69388	12563.36863		20305.17244
0	715.25	1430.5	2145.75	2861	1884	2017	2251	2800	444	1879.2	7000539	15	50	1789.01	15419908.56	5389.691912					5389.691912
0	676.5	1353	2029.5	2706	882	1025	1012	1198		1029.25	3064207	13	46	1597.71	28923828.84		4096.487082	8819.319152	19150.52286		10688.77636
0	691.75	1383.5	2075.25	2767	1145	1028	1262	1288	1356	1215.8	2957243	11.5	55	1691.21	32234808.23		9457.773845	17478.48491	8012.937004		11649.73192
0	1088.25	2176.5	3264.75	4353	1255	2460	2404	2723	1095	1987.4	9850210	16.6	81.5	2181.16	83906030.48			24092.7355	19087.70832	14645.90385	19275.44922
0	4318	8636	12954	17272	806	3199	3370	4563	4440	3275.6	59541018	18.32	41.25	1346.37	1663405411		140972.8024	101428.79	78999.06301	63825.23874	96306.47355
0	2901	5802	8703	11604	266	2341	2419	2941	1926	1978.6	27334004	13.05	17	1450.2	209656855.6	3299.758742	40965.55546			9937.595726	18067.63664
0	915	1830	2745	3660	587	982	966	1275	1127	987.4	3856817	6.97	16.33333333	1243.33	39785977.32	9507.835451	4470.081393		18633.53997		10870.48561
0	1894	3788	5682	7576		1211	1656	2087	1203	1539.25	12402576	9.13	33.33333333	1220.37	160866226.6		10497.34565	47842.83329	5360.808358		21233.66244
0	2003	4006	6009	8012	258	1678	1077	2213	2113	1467.8	13938454	10.43	38.75	1299.98	246324536.5		13872.51884	15492.37765	46863.47814	46749.42694	30744.45039
0	1656	3312	4968	6624	1184	2219	1933	2272	939	1709.4	13406158	11.81	41	1208.04	290649153.1	23843.77328	51216.53259	75682.00722	45884.78979	22763.86411	43878.1934
0	5062	10124	15186	20248	569	3729	2925	3652	520	2279	65489691	14.06	33.33333333	1430.21	444621240.2			12835.69737	39445.86864	13594.75366	21958.77322
0	3172.75	6345.5	9518.25	12691	965	1496	1670	2414	1790	1667	25867104	9.07	250	1410.36	1182663692			36308.05703	150070.2728		93189.16492
0	3815.5	7631	11446.5	15262	185	2141	1235	1563	2467	1518.2	28907259	13.14	216.6666667	1446.5	5486194666		528016.1522	414710.4798	135676.1984		359467.6101
0	1174.5	2349	3523.5	4698	336	1601	2212	2316	1057	1504.4	8300585	13.11	80	1473.21	192316294.4		19522.49374	48044.27688	55240.56935		40935.77999
0	3546.25	7092.5	10638.75	14185		1934	1824	1031	714	1375.75	25098198	12.91	237.5	1493.27	5476098454		937981.4147	463318.273	93199.81063	49694.63751	386048.534
0	5556.75	11113.5	16670.25	22227	1713	2235	1912	1745	1868	1894.6	42748212	12.71	178	1455.56	4269403514	145888.8254	210040.4096	349788.7212	27680.34996	227010.9966	192081.8605
0	910.25	1820.5	2730.75	3641	782	1821	2180	2019	1030	1566.4	6783666	12.77	166.6666667	1471.56	903742445.9		55246.80145		453731.0715	235660.2314	248212.7014
0	3199.5	6399	9598.5	12798	472	1897	2937	2848	1152	1861.2	28296914	12.66	106.6666667	1436.4	1807285187		6445.491173	376534.6351	40668.53467		141216.2203
0	3494.75	6989.5	10484.25	13979	1202	2401	2881	2938	1567	2197.8	35263735	16.44	224	1415.38	4157625543	15364.86919	244280.5662	588434.0404	483483.2496	155534.1852	297419.3821

Length	Width	Amplitude	Height range	Axgrad (°)	Axgrad (radian)	WidLen	Lenheight
1033.00	1359.00	363.00	394.00	19.36	0.34	1.32	2.62
1371.00	1331.00	390.00	537.00	15.88	0.28	0.97	2.55
1225.00	1603.00	311.00	419.00	14.25	0.25	1.31	2.92
3341.00	2890.00	354.00	411.00	6.05	0.11	0.87	8.13
2000.00	1673.00	244.00	315.00	6.96	0.12	0.84	6.35
1986.00	2479.00	104.00	349.00	3.00	0.05	1.25	5.69
1866.00	1798.00	647.00	693.00	19.12	0.33	0.96	2.69
1830.00	4194.00	416.00	534.00	12.81	0.22	2.29	3.43
627.00	636.00	125.00	169.00	11.27	0.20	1.01	3.71
3530.00	2713.00	470.00	837.00	7.58	0.13	0.77	4.22
2930.00	2723.00	770.00	892.00	14.72	0.26	0.93	3.28
2880.00	1989.00	321.00	490.00	6.36	0.11	0.69	5.88
1992.00	5975.00	636.00	697.00	17.71	0.31	3.00	2.86
1081.00	1332.00	191.00	210.00	10.02	0.17	1.23	5.15
1222.00	1341.00	212.00	328.00	9.84	0.17	1.10	3.73
2140.00	1699.00	549.00	638.00	14.39	0.25	0.79	3.35
969.00	1446.00	84.00	147.00	4.95	0.09	1.49	6.59
2087.00	1751.00	12.00	218.00	0.33	0.01	0.84	9.57
2787.00	2341.00	208.00	360.00	4.27	0.07	0.84	7.74
2293.00	1971.00	649.00	757.00	15.80	0.28	0.86	3.03
2634.00	2231.00	750.00	870.00	15.89	0.28	0.85	3.03
2923.00	2302.00	503.00	741.00	9.76	0.17	0.79	3.94
978.00	1494.00	141.00	376.00	8.20	0.14	1.53	2.60
1636.00	2231.00	470.00	603.00	16.03	0.28	1.36	2.71
2143.00	2619.00	577.00	659.00	15.07	0.26	1.22	3.25
3392.00	2506.00	448.00	512.00	7.52	0.13	0.74	6.63
1544.00	1423.00	170.00	259.00	6.28	0.11	0.92	5.96
1770.00	1262.00	308.00	420.00	9.87	0.17	0.71	4.21
995.00	2260.00	91.00	150.00	5.23	0.09	2.27	6.63
1270.00	1348.00	253.00	286.00	11.27	0.20	1.06	4.44
3610.00	1432.00	186.00	337.00	2.95	0.05	0.40	10.71
2280.00	2679.00	203.00	291.00	5.09	0.09	1.18	7.84
4870.00	2485.00	386.00	627.00	4.53	0.08	0.51	7.77
4641.00	1778.00	557.00	1032.00	6.84	0.12	0.38	4.50
3235.00	3422.00	735.00	828.00	12.80	0.22	1.06	3.91
3934.00	5055.00	373.00	603.00	5.42	0.09	1.28	6.52
2234.00	1364.00	398.00	552.00	10.10	0.18	0.61	4.05
2801.00	3891.00	854.00	1137.00	16.96	0.30	1.39	2.46
1334.00	1721.00	189.00	264.00	8.06	0.14	1.29	5.05
2157.00	5745.00	696.00	1171.00	17.88	0.31	2.66	1.84
2976.00	1479.00	581.00	640.00	11.05	0.19	0.50	4.65
4641.00	3970.00	490.00	902.00	6.03	0.11	0.86	5.15
2475.00	2008.00	278.00	417.00	6.41	0.11	0.81	5.94
1152.00	1301.00	204.00	207.00	10.04	0.18	1.13	5.57
1130.00	1512.00	135.00	172.00	6.81	0.12	1.34	6.57
2168.00	1667.00	173.00	351.00	4.56	0.08	0.77	6.18
1589.00	1471.00	347.00	370.00	12.32	0.22	0.93	4.29
1540.00	2335.00	442.00	485.00	16.01	0.28	1.52	3.18
2209.00	1510.00	293.00	341.00	7.56	0.13	0.68	6.48
2501.00	3747.00	591.00	648.00	13.30	0.23	1.50	3.86
2690.00	4361.00	201.00	337.00	4.27	0.07	1.62	7.98
831.00	1219.00	140.00	164.00	9.56	0.17	1.47	5.07
1132.00	1250.00	163.00	200.00	8.19	0.14	1.10	5.66
1172.00	1001.00	194.00	223.00	9.40	0.16	0.85	5.26
3869.00	4601.00	511.00	588.00	7.52	0.13	1.19	6.58
1474.00	1563.00	364.00	391.00	13.87	0.24	1.06	3.77
1922.00	1852.00	380.00	483.00	11.18	0.20	0.96	3.98
1673.00	1247.00	457.00	458.00	15.28	0.27	0.75	3.65
2911.00	2854.00	526.00	566.00	10.24	0.18	0.98	5.14
2041.00	2414.00	540.00	571.00	14.82	0.26	1.18	3.57
3892.00	3670.00	326.00	1058.00	4.79	0.08	0.94	3.68
5741.00	8214.00	1317.00	1665.00	12.92	0.23	1.43	3.45
3943.00	3518.00	542.00	611.00	7.83	0.14	0.89	6.45
2512.00	2260.00	292.00	344.00	6.63	0.12	0.90	7.30
2857.00	2397.00	363.00	454.00	7.24	0.13	0.84	6.29

Table 6. All measured parameters for Dawes crater valleys and valley heads

Crater 1 valleys and valley heads

Length 0% (m)	Length 25%	Length 50%	Length 75%	Length 100%	Width 0% (m)	Width 25%	Width 50 %	Width75%	Width 100%	Average Width	Surface (m²)	Slope (°)	Depth (m)	Elevation (m)	Cumulative volume (m^3)	Cross-section 0 %(m²)	Cross-section 25%	Cross-section50%	Cross-section 75%	Cross-section 100%	Average cross-section
0	726	5808	2178	2904	1224	1432	1088	1099	912	1151	356222	3.55	30	1647	19131853.45		2605.845272	8545.037367	8613.428776		6588.103805
0	792	6336	2376	3168		800	1210	2093	797	1225	385117	3.67	14.33333333	1796	10555244.18		3078.116128	4454.805546	2462.574709		3331.832128
0	961	7688	2883	3844	513	781	1063	1214	335	781.2	348014	3.54	18.66666667	2029	27191703.34		9795.119843	1213.072441	10213.22031		7073.804198
0	871	6968	2613	3484	1007	1215	1499	1527		1312	479228	2.94	9	2449	6506254.623	1445.552649		2289.381119			1867.466884
0	792	6336	2376	3168	783	1437	1303	1372	680	1115	384297	3.99	31.66666667	1977	30542578.32	3115.40572	12837.22105	8277.115409	14334.11933		9640.965379
0	735	5880	2205	2940	572	1186	1740	1366	672	1107.2	371584	4	27	2139	37492390.38	5982.372395	6493.263624	27232.70563	12650.27271	11403.95431	12752.51373
0	414	3312	1242	1656		1495	1705	1607	1343	1537.5	257441	4	37	2162	29477785.17	15647.8365	10693.5004	20903.0661	20682.62765	21075.9439	17800.59491
0	918	7344	2754	3672	1384	1857	2319	2519	1905	1996.8	746417	3.33	25	1403	110828607.3	3792.590665			56571.57452		30182.08259
0	1465	11720	4395	5860		2059	1786	1846		1897	122318	2.93	45	2559	207044773.1	11408.25158	59255.49349				35331.87254
0	3216	25728	9648	12864	504	1969	1062	1823	792	1230	192535	3.29	15	1625	104180056.4		12893.91546	4055.762865	7346.043778		8098.574035
0	1496	11968	4488	5984		932	1360	1304		1198.666667	698934	3.43	19.5	1787	24777473.79		7082.821231		1198.42001		4140.620621
0	1549	12392	4647	6196		448	547	760	889	661	369327	3.27	13.75	1886	28618748.72		8484.673634	1461.315344	2763.956869	5765.682764	4618.907153
0	751	6008	2253	3004	969	1108	972	1172		1055.25	311415	3.77	27.5	2434	36234016.33		13625.77207	10173.97299	13700.03327	10747.91319	12061.92288
0	1045	8360	3135	4180	983	828	655	928		848.5	344379	4.29	32.5	2337	35117923.3		13518.93892		3283.895199		8401.417057
0	991	7928	2973	3964	711	990	1090	875		916.5	389462	4.56	23.33333333	2364	30038198.92		4829.88208	10983.32171	6920.044634		7577.749475
0	636	5088	1908	2544		535	656	915	932	759.5	162585	3.96	18	2546	9872399.304		3286.968047	5906.918425	2448.09384		3880.660104
0	542	4336	1626	2168	500	752	930	981	893	811.2	184532	4.53	15.66666667	2359	13960385.7	38.20816112	4605.615438		14674.05329		6439.292297
0	1523	12184	4569	6092	238	1253	1298	1532		1080.25	812977	5.87	48.33333333	1582	96240503.45		4169.063668	15659.72967	27564.75727		15797.8502
0	532	4256	1596	2128	1058	586	516	594	630	676.8	124376	3.78	12.5	2238	4943872.804		1594.535421		3051.961576		2323.248498
0	1544	12352	4632	6176	1324	1083	1304	1850	1753	1462.8	936943	4.56	37.5	1858	95915340.7	14203.7456	30565.72789	11004.52375	6347.337417		15530.33366
0	1590	12720	4770	6360	874	1248	979	882		995.75	766515	4.68	38.33333333	1960	103751993.6	24535.35866	17542.62649			6861.634471	16313.20654
0	915	7320	2745	3660	225	929	925	771	565	683	292720	4.06	21.66666667	2290	33018670.01		5044.66951	11469.52484	10550.28926		9021.494538
0	773	6184	2319	3092	920	1013	1642	2144		1429.75	435590	4.84	21.66666667	2421	33724589.12		15097.82644	8338.991471		9284.322892	10907.04693
0	886	7088	2658	3544	1175	1642	1912	2057		1696.5	615958	4.05	14.4	2242	24476263.44	8551.089879	11691.73165	5074.490226	6596.590757	2618.071867	6906.394876
0	1460	11680	4380	5840	1790	2435	3612	3537	1162	2507.2	162663	3.95	27.33333333	2016	200278415.7		9071.979378	41250.32226	52560.44613		34294.24926
0	1071	8568	3213	4284	871	2344	2615	2521	3017	2273.6	105619	4.16	63.33333333	2151	400191923.4		71081.02045	69943.14501	139222.2795		93415.48165
0	1214	9712	3642	4856	1355	1353	2028	1926	405	1413.4	907905	3.46	10	2448	24201248.15	3187.876191		6779.688943			4983.782567
0	833	6664	2499	3332	1128	1852	1109	1332		1355.25	427196	4.6	32	2086	48495908.9	12489.62155	25492.3123	3150.174996	17086.26919		14554.59451
0	561	4488	1683	2244	659	855	1146	776	507	788.6	184616	3.48	17	1870	19575835.41			8723.63432			8723.63432
0	2501	20008	7503	10004	803	942	2141	1789	530	1241	168655	3.17	13.5	2326	54689915.64	3041.442302	1514.135332	11509.34952	5802.292208		5466.804842
0	531	4248	1593	2124	1681	1923	1728	1531	324	1437.4	350005	3.76	16.75	2725	19385332.73	14573.3187	10092.39221	5555.245217	6286.261826		9126.804487
0	368	2944	1104	1472	1081	822	815	790		877	118779	4.65	15.75	2749	8747871.178	12399.84484	5548.675166	4090.5607	1732.308364		5942.847268
0	495	3960	1485	1980	281	1356	1548	1632	364	1036.2	281194	4.66	10.66666667	2751	6057141.824	3269.564586		3991.108412		1916.814614	3059.162537

Length	Width	Amplitude	Height range	Axgrad (°)	Axgrad (radian)	WidLen	Lenheight
3383.00	1970.00	386.00	686.00	6.51	0.11	0.58	4.93
2091.00	2316.00	748.00	751.00	19.68	0.34	1.11	2.78
3421.00	2462.00	894.00	944.00	14.65	0.26	0.72	3.62
1917.00	2540.00	253.00	343.00	7.52	0.13	1.32	5.59
1744.00	1434.00	237.00	588.00	7.74	0.14	0.82	2.97
1997.00	2044.00	338.00	373.00	9.61	0.17	1.02	5.35
1191.00	1682.00	143.00	372.00	6.85	0.12	1.41	3.20
1320.00	1828.00	428.00	425.00	17.96	0.31	1.38	3.11
1423.00	1999.00	475.00	648.00	18.46	0.32	1.40	2.20
1389.00	3108.00	436.00	666.00	17.43	0.30	2.24	2.09
934.00	690.00	363.00	392.00	21.24	0.37	0.74	2.38
1562.00	2080.00	122.00	369.00	4.47	0.08	1.33	4.23
1591.00	1441.00	351.00	531.00	12.44	0.22	0.91	3.00
1085.00	1041.00	309.00	431.00	15.90	0.28	0.96	2.52
1583.00	1357.00	477.00	500.00	16.77	0.29	0.86	3.17
4795.00	4292.00	1579.00	1595.00	18.23	0.32	0.90	3.01
5568.00	6187.00	1529.00	1595.00	15.36	0.27	1.11	3.49
1718.00	3064.00	297.00	317.00	9.81	0.17	1.78	5.42
4065.00	3942.00	266.00	333.00	3.74	0.07	0.97	12.21
1643.00	1224.00	521.00	538.00	17.59	0.31	0.74	3.05
1960.00	1717.00	493.00	626.00	14.12	0.25	0.88	3.13
1510.00	1489.00	398.00	528.00	14.77	0.26	0.99	2.86
2482.00	2582.00	483.00	540.00	11.01	0.19	1.04	4.60
1264.00	921.00	326.00	316.00	14.46	0.25	0.73	4.00

Table 7. All measured parameters for Crater 1 valleys andvalley heads

Moutain 1 valleys

Length 0% (m)	Length 25%	Length 50%	Length 75%	Length 100%	Width 0% (m)	Width 25%	Width 50 %	Width75%	Width 100%	Average Width	Surface (m²)	Slope (°)	Depth (m)	Elevation (m)	Cumulative volume (m^3)	Cross-section 0 %(m²)	Cross-section 25%	Cross-section50%	Cross-section 75%	Cross-section 100%	Average cross-section
0	2499	4998	7497	9996	773	1777	2920	3475	5314	2851.8	27226319	5.08	178	3075.5	1046767511	33233.93315	64164.65529	203129.971	118345.9947		104718.6385
0	[illegible]	1590.6635	2385.99525	3181.327	1256	1998	2077	2316	2053	1940	6709237	5.86	163	2620.6	100344421.6		49875.61612	23497.35279	20356.39578	32437.38477	31541.68736
0	[illegible]	2517.3705	3776.05575	5034.741	1212	1227	1840	2538	2574	1878.2	9252865	4.81	151	2840.4	230333708.6			65839.69816	25658.04069		45748.86942
0	[illegible]	1855.7925	2783.68875	3711.585		1949	1984	1956	1951	1960	7411431	2.83	139.2	1673.9	62419854.04			17348.61521	21023.97419	12080.13151	16817.57363
0	915.685	1831.37	2747.055	3662.74	577	1425	1858	1574		1358.5	5187937	7.09	127	1872.8	128046098.2	13701.08849	37811.71891	47081.68494	41241.91235		34959.10117
0	864.446	1728.892	2593.338	3457.784	1293	1119	1157	1129	871	1113.8	3770841	5.45	142	2307.8	137494329.7	44333.18425	38465.53533	35883.97916	45104.5915	35031.27341	39763.71273

Table 8. All measured parameters for Moutain 1 valleys

Length 0% (m)	Length 25%	Length 50%	Length 75%	Length 100%	Width 0% (m)	Width 25%	Width 50 %	Width75%	Width 100%	Average Width	Surface (m^2)	Slope (°)	Depth (m)	Elevation (m)	Cumulative volume (m^3)	Cross-section 0 %(m^2)	Cross-section 25%	Cross-section50%	Cross-section 75%	Cross-section 100%	Average cross-section
0	2154	4308	6462	8616	564	1954	2303	2034	1392	1649.4	15222055	22	418.5	2682	5244604149		434519.7395	536767.5385	379418.6488	1084114.941	608705.2169
0	295	590	885	1180	532	500	632	533	511	541.6	637286	36	118.25	3200	38367479.47		38138.64134	30264.65153	19631.16289	42024.79666	32514.81311
0	163	326	489	652	544	483	363	366	279	407	270680	53	91.66666667	3490	12455319.22	16464.36252	23214.39558	17630.99292			19103.25034
0	1966	3932	5898	7864	1525	2028	2757	2415	2345	2214	16762193	30	610.75	2264	6147119372		427389.3336	1045665.688	691548.4565	962110.343	781678.4553
0	352	704	1056	1408	616	719	1020	835	951	828.2	1084809	30	56	2747	39594054.3		28120.7772				28120.7772
0	1266	2532	3798	5064	1995	4050	1845	1552	839	2056.2	12783682	27	458.3333333	2687	3753900155	830681.2222	693724.9972		699468.28		741291.4998
0	1284	2568	3852	5136	789	1195	1826	717	1024	1110.2	5848886	29	150	2394	449750489.5		52563.08763			122573.3958	87568.24173
0	770	1540	2310	3080	1671	1466	1330	1362	1912	1548.2	4315225	37	276	2225	555429669.8	69277.09103	322528.3031	266590.8099	62941.02939		180334.3084
0	242	484	726	968	1600	1314	1495	1372	545	1265.2	1623056	38	396.75	1982	195965716.2	95452.48156	200565.727	299629.0452	358506.986	58065.36855	202443.9217
0	748	1496	2244	2992	405	411	1106	1014	415	670.2	2244964	37	173	2353	378841716.7		17151.77842	210840.9839	151861.9001		126618.2208
0	5103	10206	15309	20412	1712	6211	4021	5430	4337	4342.2	97240464	26	849.8	1567	50628826386	658617.7049	2748606.571	4838113	2996417.26	1159976.404	2480346.188

Table 9. All measured parameters for Chamonix valleys

	Bakhuysen crater	GLF-crater	Dawes crater	Mountain 1	Crater 1	Chamonix
Number of valleys identified	36	23	42	6	33	13
Average length (km)	10	4.2	4.4	5	3.8	4.7
Average width (km)	0.5	1.2	2	1.8	1.3	1.5
Average aspect ratio length:width	21.5	3.7	2.4	2.7	2.9	3.2
Average elevation (m)	170	1280	1600	2200	2150	2500
Average depth (m)	15	20	56	143	25	308
Average cross-sectional area (m^2)	6537	12647	24568	45591	13631	480793
Average V-index	0.07	0.15	0.20	0.21	0.23	0.21

Table 10. Average values for each measured parameter for valleys in each studied zone.

	Dawes crater	Crater 1	Evans and Cox (2017)	Barr and Spagnolo (2015)
Number of valley heads identified	75	25	1593	10362
Average width (m)	2398	2177	656	749
Average length (m)	2317	2120	625	744
Average amplitude (m)	388	493	260	
Average altitudinal range (m)	519	452	310	309
Average size (m)	1377	1242		
Average width to length ratio	1.05	1.02	1.05	1.03
Lip average height (m)	75	35		
Average axgrad (°)	9.97	13.18	23.1	24.2
Average length to height ratio	4.94	3.87	2.03	2.58
Number of valley head linked with the valley	41	13		

Table 11. Average values for each of the measured parameters for valley heads in each of studied areas and average values from terrestrial cirque from Barr and Spagnolo (2015); Evans and Cox (2017)

n1\n2	2	3	4	5	6	7	8	9	10	11	12	13	14	15	16	17	18	19	20
2																		0	0
3								0	0	0	1	1	1	2	2	2	2	3	3
4					0	0	1	1	2	2	3	3	4	5	5	6	6	7	8
5				0	1	1	2	3	4	5	6	7	7	8	9	10	11	12	13
6			0	1	2	3	4	5	6	7	9	10	11	12	13	15	16	17	18
7			0	1	3	4	6	7	9	10	12	13	15	16	18	19	21	22	24
8			1	2	4	6	7	9	11	13	15	17	18	20	22	24	26	28	30
9		0	1	3	5	7	9	11	13	16	18	20	22	24	27	29	31	33	36
10		0	2	4	6	9	11	13	16	18	21	24	26	29	31	34	37	39	42
11		0	2	5	7	10	13	16	18	21	24	27	30	33	36	39	42	45	46
12		1	3	6	9	12	15	18	21	24	27	31	34	37	41	44	47	51	54
13		1	3	7	10	13	17	20	24	27	31	34	38	42	45	49	53	56	60
14		1	4	7	11	15	18	22	26	30	34	38	42	46	50	54	58	63	67
15		2	5	8	12	16	20	24	29	33	37	42	46	51	55	60	64	69	73
16		2	5	9	13	18	22	27	31	36	41	45	50	55	60	65	70	74	79
17		2	6	10	15	19	24	29	34	39	44	49	54	60	65	70	75	81	86
18		2	6	11	16	21	26	31	37	42	47	53	58	64	70	75	81	87	92
19	0	3	7	12	17	22	28	33	39	45	51	56	63	69	74	81	87	93	99
20	0	3	8	13	18	24	30	36	42	46	54	60	67	73	79	86	92	99	105
21	0	3	8	14	19	25	32	38	44	51	58	64	71	78	84	91	98	105	112
22	0	4	9	14	21	27	34	40	47	54	61	68	75	82	89	96	104	111	118
23	0	4	9	15	22	29	35	43	50	57	64	72	79	87	94	102	109	117	125
24	0	4	10	16	23	30	37	45	52	60	68	75	83	91	99	107	115	123	131
25	0	5	10	17	24	32	39	47	55	63	71	79	87	96	104	112	121	129	138
26	0	5	11	18	25	33	41	49	58	66	74	83	92	100	109	118	127	135	144
27	1	5	12	19	27	35	43	52	60	69	78	87	96	105	114	123	132	142	151
28	1	5	12	20	28	36	45	54	63	72	81	91	100	109	119	128	138	148	157
29	1	6	13	21	29	38	47	56	66	75	85	94	104	114	124	134	134	144	164
30	1	6	13	22	30	40	49	58	68	78	88	98	108	119	129	139	150	160	170
31	1	6	14	22	32	41	51	61	71	81	92	102	113	123	134	145	155	166	177
32	1	7	14	23	33	43	53	63	74	84	95	106	117	128	139	150	161	172	184
33	1	7	15	24	34	44	55	65	76	87	98	110	121	132	144	155	167	179	190
34	1	7	16	25	35	46	57	68	79	90	102	113	125	137	149	161	173	185	197
35	1	8	16	26	37	47	59	70	82	93	105	117	129	142	154	166	179	191	203
36	1	8	17	27	38	49	60	72	84	96	109	121	134	146	159	172	184	197	210
37	1	8	17	28	39	51	62	75	87	99	112	125	138	151	164	177	190	203	217
38	1	9	18	29	40	52	64	77	90	102	116	129	142	155	169	183	196	210	223
39	2	9	19	30	41	54	66	79	92	106	119	133	146	160	174	188	202	216	230
40	2	9	19	31	43	55	68	81	95	109	122	136	150	165	179	193	208	222	237

Table 12. Mann-Whitney table for a bilateral test.

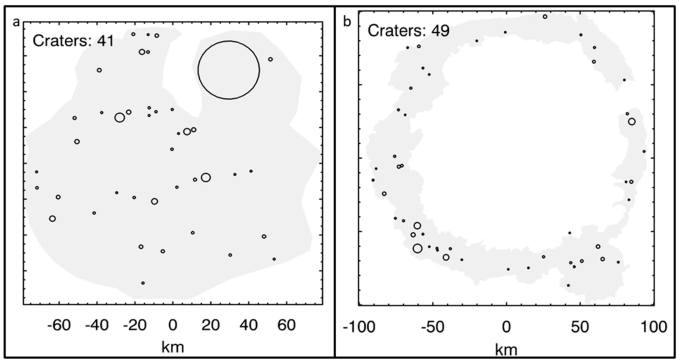

Fig. 21. Map of the count-areas of craters > 1km in Dawes crater. (a) Dawes crater floor. (b) Dawes crater inner walls.

Mars

Earth

Morphometric evidence of 3.6 Ga glacial valleys and glacial cirques in martian highlands: south of Terra Sabaea

- Early Mars
- Glacial landscape
- Morphometric comparison

- Morphological parameters
- Geometrical parameters
- Comparison with Mars

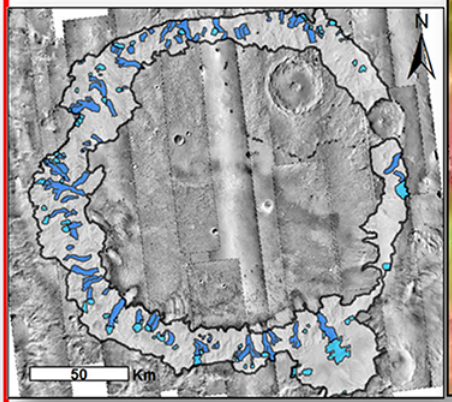

Dawes crater

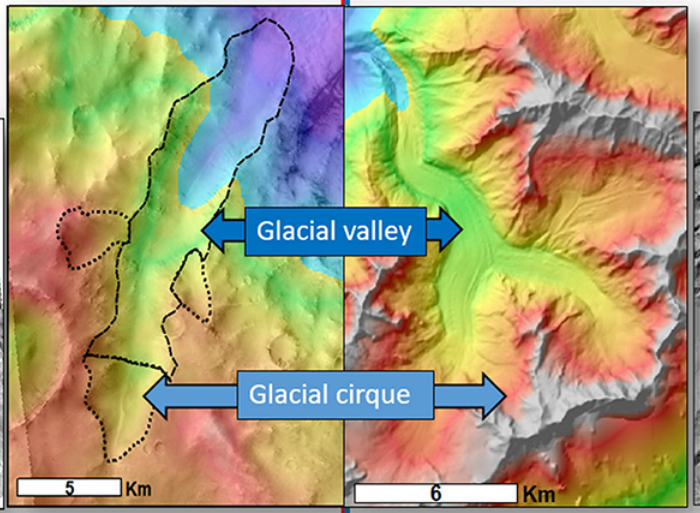

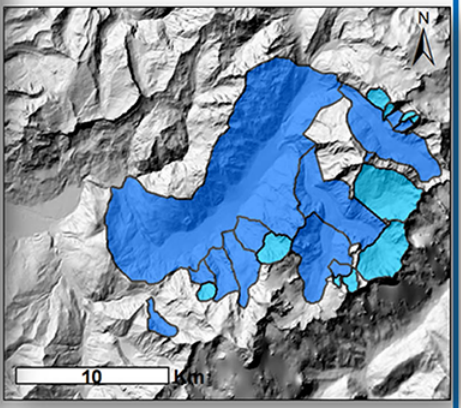

Chamonix valley